GEORG-AUGUST-UNIVERSITÄT
GÖTTINGEN

Fakultät für
Physik

Master's Thesis

# Charakterisierung hochbestrahlter polykristalliner Diamantsensoren für ionisierende Strahlung

# Characterisation of highly irradiated polycrystalline diamond sensors for ionising radiation


prepared by

**Lars Graber**

from Helmstedt

at the II. Physikalischen Institut



| | |
|---|---|
| **Thesis number:** | II.Physik-UniGö-MSc-2011/01 |
| **Thesis period:** | 14th March 2011 until 13th September 2011 |
| **Supervisor:** | Dr. Jens Weingarten |
| **First referee:** | Prof. Dr. Arnulf Quadt |
| **Second referee:** | Priv.Doz. Dr. Jörn Große-Knetter |

# Zusammenfassung

Hochbestrahlte Diamanten wurden auf ihre Eignung im Bezug auf die Verwendung als Sensormaterial für Spurdetektoren untersucht. Hierfür wurden zwei Teststationen für C-V und CCD-Messungen aufgebaut. Es zeigt sich, dass für hochbestrahlte Diamanten eine Abhängigkeit der Kapazität von der angelegten Spannung besteht. Messungen der CCD sind sowohl bei sehr niedriger CCD als auch für einen großen Spannungsbereich mit hoher Präzision möglich. Graphitisierung von Diamant mittels eines Femtosekundenlasers wurde zur Herstellung von Elektroden im Material für 3D-Sensoren untersucht.

**Stichwörter:** Hochenergiephysik, Diamant, Halbleitersensoren

# Abstract

Highly irradiated diamonds are studied for their use as sensors for tracking detectors. Two different setups for C-V and CCD measurement were built. For highly irradiated diamonds a change of the capacitance with respect to the bias voltage is observed. Measurements of very low values of CCD are possible over a wide voltage range with high statistical precision. Graphitisation of diamond using a femtosecond laser is tested for the manufacturing of electrodes for 3D sensors.

**Keywords:** high energy physics, diamond, semiconductor sensors

# Contents

# Nomenclature

## Acronyms

| abbreviation | meaning |
|---|---|
| m.i.p. | minimum ionising particle |
| DUT | device under test |
| CCD | charge collection distance |
| CVD | chemical vapor deposition |
| scCVD | singlecrystalline diamond |
| pCVD | polycrystalline diamond |

# 1. Introduction

Tracking detectors are an important part of every multipurpose particle physics detector, especially at hadron colliders, for example the Large Hardon Collider (LHC). As the number of particles increases with the center of mass energy, the requirements on detectors have increased, too. They have to have a high granularity, which means better spatial resolution. Silicon has been the material of choice for most tracking detectors for the past decades, but may be at its limits. Increasing particle flux causes significant damage in the sensor and limits its lifetime.
Diamond sensors are an alternative for the harshest environments. Diamond is very radiation hard due to the high displacement energy and has similar properties compared to silicon. The amplitude of the signal is lower than in Silicon, as it has a larger band gap. But due to this larger band gap the overall noise level is lower. Thus diamond sensors are an option for the innermost layer of a future tracker at the upgrade of the LHC, the so called super LHC (sLHC).
During operation the sensors will be exposed to very high radiation doses. This will damage the bulk and especially decrease the charge collection efficiency. Thus their behaviour at the end of their lifetime has to be studied.
In this thesis studies for highly irradiated samples are presented. For information about the damage inside the bulk the change of capacitance with respect to the bias voltage is determined. The charge collection distance (CCD), a figure of merit which is connected to the charge collection efficiency, is measured for different samples. For this measurement a setup is built which has a very low noise level. To increase this efficiency, new sensor concepts like 3D sensors are an option. First steps for the fabrication of electrodes of such sensors, using a femtosecond laser to graphitise the diamond, are presented.
In Chapter 2 an overview of the mode of operation of solid state tracking detectors is presented. Chapter 3 explains the special properties of diamond if used as a sensor. The principle of 3D sensors and the options to manufacture them in diamond are explained in Chapter 4. Measurements of the capacitance of irradiated diamond samples with respect to the bias voltage are presented in Chapter 5. The results of the CCD measurement are given in Chapter 6. In Chapter 7 the first results of the graphitisation of diamond are

described.

# 2. Principles of solid state particle detectors

## 2.1. Energy loss of particles

Particles traversing matter interact with it and thus loose energy. This energy loss happens for a heavy charged particle mainly in three ways [1]:

- ionisation or excitation
- Cherenkov radiation
- transition radiation in inhomogeneous materials

For solid state detectors, such as silicon or diamond sensors, ionisation is the main process. Ionisation in a solid state detector means the creation of electron-hole pairs. The amount $n_{e/h}$ of pairs can be calculated via

$$\langle n_{e/h} \rangle = \frac{\Delta E}{W}$$

where $\Delta E$ is the total deposited energy and $W$ the average energy needed to create one electron-hole pair. The energy depends on the band gap between the highest band which is filled with electrons and the lowest empty band called valence and conduction band, respectively. This is an intrinsic parameter of semiconductors. However, only for direct semiconductors the band gap equals the energy needed to create an electron-hole pair. Direct means that an electron can switch from the valence band to the conduction band without having to change its momentum. If the band gap is indirect, like in silicon and diamond, the highest possible state in the valance band and the lowest possible state in the conduction band require different momenta. A change of the momentum of the electron increases the energy needed to create an electron-hole pair.
The average of the deposited energy $\Delta E$ can be calculated using the Bethe-Bloch formula [2]. It describes the mean energy loss of heavy charged particles, i.e. all charged

| | |
|---|---|
| $v$ | velocity of the incident particle |
| $c$ | speed of light |
| $\beta$ | $v/c$ |
| $\gamma$ | $(1-\beta^2)^{-1/2}$ |
| $r_e$ | classical electron radius |
| $m_e$ | electron mass |
| $N_a$ | Avogadro's number |
| $I$ | mean excitation potential |
| $Z$ | atomic number of the absorbing material |
| $A$ | atomic weight of the absorbing material |
| $\rho$ | density of the absorbing material |
| $z$ | charge of the incident particle |
| $W_{max}$ | maximum energy transfer in a single collision |

***Table 2.1.:*** Explanation of symbols used in Equation 2.1.

particles except electrons and high energy muons. For these Bremsstrahlung dominates.

$$-\left\langle \frac{dE}{dx} \right\rangle = 2\pi N_a r_e^2 m_e c^2 \rho \frac{Z}{A} \frac{z^2}{\beta^2} \left[ \ln\left( \frac{2m_e\gamma^2 v^2 W_{max}}{I^2} \right) - 2\beta^2 \right] . \tag{2.1}$$

The symbols used in this equation are explained in Table 2.1. It is possible to express this formula as a function of the relativistic parameters $\beta\gamma$. An example is given in Figure 2.1 for the energy loss of muons in Copper. It shows that the Bethe-Bloch formula cannot describe the energy loss for every $\beta\gamma$ of the muon. At a $\beta\gamma$ greater than 1000 losses due to Bremsstrahlung are dominating. For a $\beta\gamma$ lower than 0.1 energy is lost due to nuclear reactions.

An important aspect to note is that $\langle \mathrm{d}E/\mathrm{d}x \rangle$ only gives the mean energy loss. For thin sensors the energy loss follows a Landau-distribution. So the mean value does not equal the most probable value which is significantly lower. An example for this is given in Figure 2.2 for a minimum ionising particle (m.i.p.) in silicon. The minimum of the Bethe-Bloch formula is located at a $\beta\gamma$ of approximately four. As the energy loss increases only slightly for higher $\beta\gamma$ before reaching a plateau, all particles with $\beta\gamma$ above four are called m.i.p.. Their energy corresponds to the minimal loss of energy due to ionisation effects. So a m.i.p. generates the lowest signal in a detector.

Electrons lose energy mainly through Bremsstrahlung. The loss is directly proportional to the energy $E$ of the incoming particle

$$-\frac{\mathrm{d}E}{\mathrm{d}x} = \frac{E}{X_0} .$$

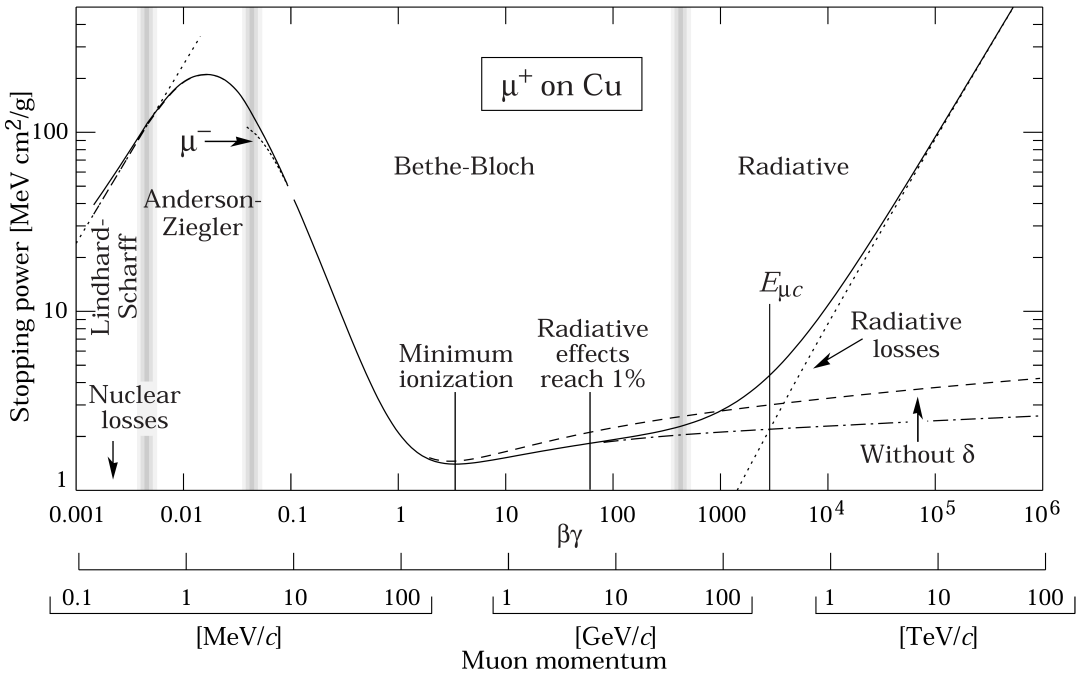


***Figure 2.1.:*** Energy loss of muons in Copper [3].

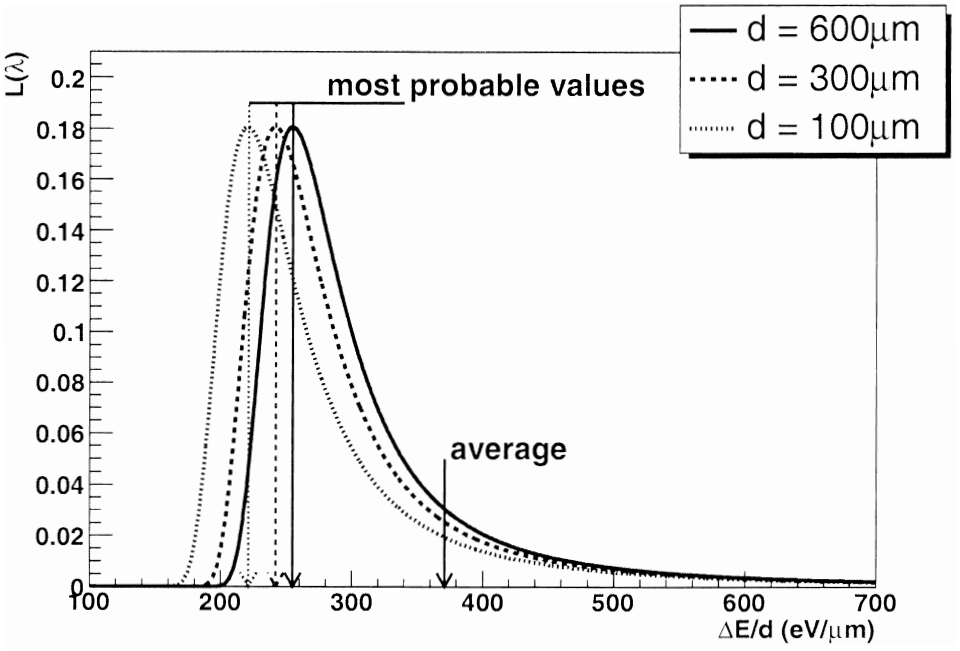


***Figure 2.2.:*** Example for the Landau-distribution $L(\lambda)$ of the energy loss of a m.i.p. in silicon with thickness $d$. The energy loss has been normalised to the sensor thickness $d$. The mean value and most probable values are indicated [4].

$X_0$ is a material specific parameter called radiation length. It describes the mean distance at which an electron has only $1/e$ of its original energy left.
Photons interact with matter in different ways. These are:

- photo effect
- Compton effect
- pair production

The cross section of each process depends on the energy of the photon and on the material. For a typical high energy photon in tracking detectors only pair production is important. In this process the photon transforms into an electron-positron pair. This means that the whole energy of the photon is deposited in this process and thus in the detector at once. Uncharged massive particles cannot interact with matter through the electromagnetic force due to their missing charge. Their only interaction process is scattering. In this process electrons or atoms of the sensor material may be excited and their relaxation can be measured.

## 2.2. Sensor design

As the radiation length of Silicon and diamond is rather long, see Table 3.1, their stopping power is very weak. Especially compared to those of e.g. Iron with a radiation length of 1.76 cm [3]. Thus semiconductors are used to build tracking detectors and not calorimeters. The purpose of a tracking detector is not to measure the full energy of a particle but to determine its trajectory through a magnetic field. With this information the ratio of charge to momentum of the particles can be calculated.
Electrons of an atom have discrete energy levels. In a crystal lattice these energy levels cannot have the same value for each atom due to the Pauli exclusion principle. Thus the energy levels for each atom shift to slightly lower or higher values compared to a single atom. This creates the so called energy bands in a solid state body. The energy difference between the highest filled and the lowest unfilled band is called band gap. If there is no band gap, the solid state body is a conductor. Semiconductors have values below 4 eV. Materials with higher band gaps are insulators.
Silicon has a band gap of 1.12 eV and is thus a semiconductor. Due to the small band gap, at room temperature single electrons in the valence band have enough energy to cross the gap. This creates an electron in the conduction band and a hole in the valence band. Both of them can be used as charge carriers. Thus the resistivity for intrinsic Silicon is

rather low with $2.3 \cdot 10^5$ Ωcm. If a potential is applied this leads to a significant leakage current. A high leakage current is disfavoured as the shot noise of a sensor is proportional to the square root of it. For intrinsic silicon this noise is easily in the order of the detected signal.

Thus for semiconductors p-n-junctions are used which consist of two differently doped semiconductors. Doping means the inclusion of foreign atoms in the crystal lattice of an intrinsic semiconductor. These atoms either have an electron more or less on the outermost orbit than the semiconductor. They are called donators or acceptors and the materials n- or p-doped, respectively. Donators introduce new energy states with slightly lower energies than the conduction band in the band gap. Acceptors also generate new energy states but with energies slightly higher than the valence band. In thermal equilibrium at room temperature these states are completely ionised.

For a p-n-junction these two doped semiconductors are merged. At the border of these materials the positive and negative charges cancel out. This results in an effective space charge in this region. It is either positive or negative for p- or n-doped material, respectively. This region is called depletion zone. The thickness of this zone can be expanded by reverse biasing the junction. Typically the doping concentration of the two materials differs by orders of magnitude so that the depletion region expands nearly exclusively into the lower doped semiconductor. The potential to completely deplete a sensor is the depletion voltage.

The positive and negative space charge induce an electric field in the depletion zone. If an electron-hole pair is created in this region the charge carriers will move in opposite directions. This prevents their recombining. Thus deposited charge can only be collected in this depleted zone. It is therefore crucial to deplete the whole sensor.

Radiation can damage the crystal lattice and generate e.g. vacancies and interstitials. These defects may introduce new energy states in the band gap and thus contribute to the effective doping of a sensor. As more p-doping like defects are created than n-doping like the effective doping changes with increasing radiation dose. For a n-doped material this can lead to a type inversion. As the doping concentration increases, the depletion voltage increases, too. At high radiation doses it might be so high that the sensor cannot be fully depleted anymore. This leads to a loss of efficiency.

The p-n-junction significantly increases the resistivity of the sensor and thus decreases the leakage current and shot noise to an acceptable level.

For diamond, being an insulator, no doping is needed as its intrinsic resistivity is very high. Thus undoped diamond is used as sensor material. A sketch of a diamond detector can be seen in Figure 2.3. Essentially it is a drift chamber. For semiconductors the

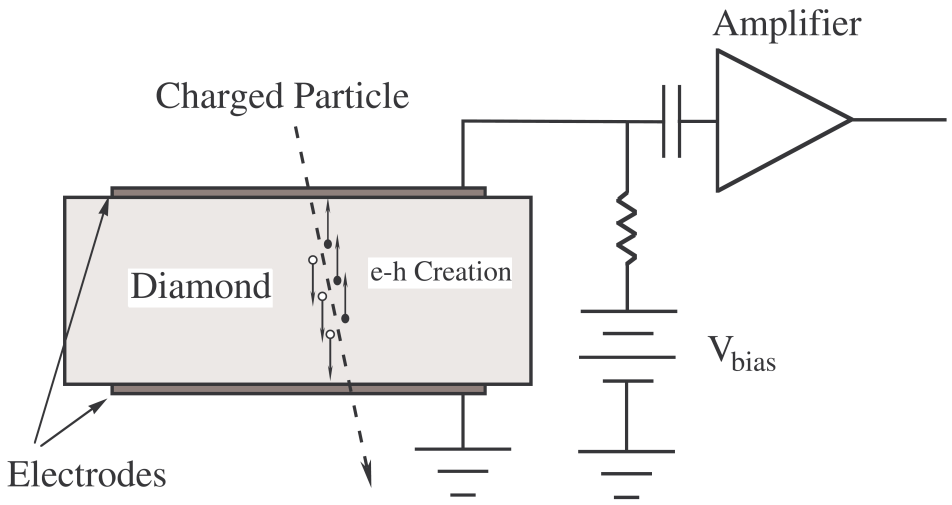


***Figure 2.3.:*** Schematic illustration of a diamond detector with the first part of the electronic read-out. As the bias voltage is connected to the same electrode as the read-out, the capacitor decouples the amplifier from it [5].

concept is the same but with a p-n-junction. This junction is reverse biased to create a depletion zone for charge collection. In diamond such a special zone is not needed as there are no intrinsic free charge carriers. Thus it does not matter in which direction the voltage is applied which means that both types of charge carriers, electrons and holes, can be collected with the same sensor by just switching the sign of the electric field. Due to the fact that no depleted zone has to be created by the potential, the bias voltage can be the same even after irradiation without any drop in efficiency.

## 2.3. Read-out chain

To read-out a sensor the charges have to be collected. For this an electric field has to be applied to the diamond. Because of it, the electrons and holes drift to the electrodes. This drift induces a charge on the electrodes. The instantaneous induced charge $i_k$ is given by Ramo's theorem [6]:

$$i_k = q\vec{v}\vec{E}_W \ . \tag{2.2}$$

$\vec{v}$ denotes the drift velocity of the charges, $q$ the total deposited charge and $\vec{E}_W$ the weighting field, which can be derived from the geometry of the electrodes and the applied voltage. To obtain the total collected charge $Q$, this equation has to be integrated until

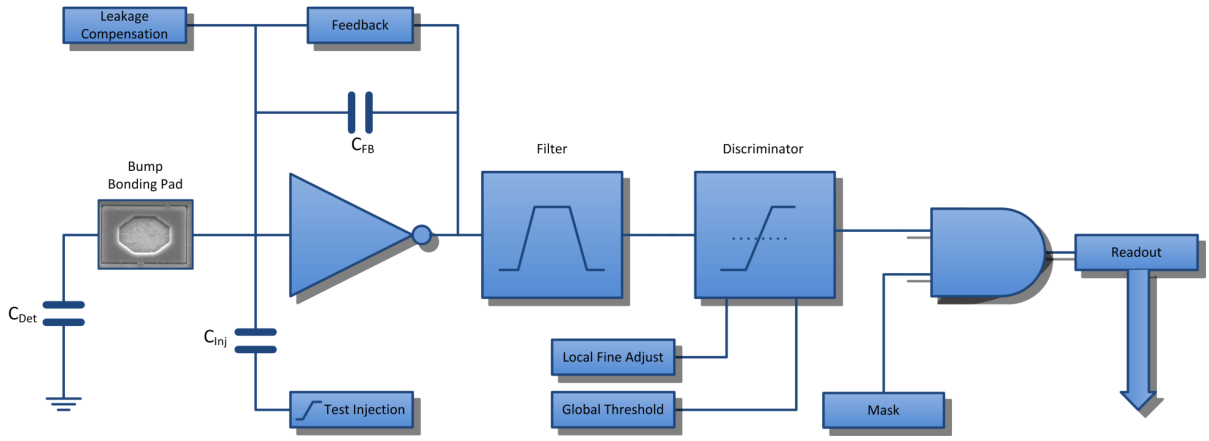


***Figure 2.4.:*** Scheme of the electronics of a typical hybrid pixel cell. The sensor is represented by $C_{Det}$.

charge collection is complete

$$Q = \int i_k \, \mathrm{d}t \; .$$

In electronic circuits this is done by the current charging a capacitor, the so called feedback capacitor. It is connected parallel to a charge sensitive amplifier. The potential difference on its in- and output is amplified. This resulting voltage can be further progressed.
A scheme of such a read-out chain is illustrated in Figure 2.4. This is the typical design for a pixel cell of a hybrid pixel detector. Hybrid means that the sensor and the read-out electronics are on two different chips. The sensor and the read-out chip are connected via a bump bond for each pixel cell. The advantage of this approach is the ability to design the sensor and electronics independently and to connect each pixel cell to individual read-out electronics. This and the low manufacturing costs due to separated sensor and electronic chips make this design the common choice for pixel detectors at hadron colliders.
The collected charge from the detector is gathered in the feedback capacitor $C_{FB}$. The resulting voltage difference at a parallel connected charge sensitive amplifier is amplified. To discharge the feedback capacitor either a resistor or a current source is connected in parallel. This discharging is needed as otherwise the charges from multiple hits would add up. The time constant of this process is a crucial parameter as it has influence on the voltage output of the amplifier and thus on the measured charge. It should be long enough to discharge the feedback capacitor as less as possible during charge collection. This error is called ballistic deficit. But the time constant also has to be short enough to prevent the pile-up of several hits.

The signal is often further processed through a filter. This band-pass shapes the signal and reduces the noise by attenuating low and high frequencies. Thus it is crucial to know the charge collection time of the sensor and choose the passband accordingly.
For digitisation the next step is a discriminator. As long as the signal exceeds a threshold the output is a digital one, otherwise it is zero. If the threshold is high enough this step further reduces the noise. For adjustment it can be controlled globally as well as for each pixel cell individually. The output can either be read out directly from a buffer or sampled with a clock to determine the start and end of a signal.

# 3. Diamond as a sensor material for particle detectors

## 3.1. Production of CVD diamond

Using natural diamonds for large scale particle detectors is impossible due to their shape, weight and price. Natural diamonds found in mines or elsewhere tend to be small and light, i.e. less than a gram. Their shape is irregular and roughly spherical. For a particle detector the sensor material needs to be thin in one direction and reasonably thick in the other two. Because of its lower price, only synthetic diamonds are an option.
The most rudimentary approach for manufacturing diamonds is exposing Carbon atoms to high pressure. One of the first to synthesise diamonds with this method was Hall in 1954 [7, 8]. However, with sizes of a few millimeters these diamonds are too small for detector purposes.
Today the most common way to produce large diamond samples is chemical vapor deposition (CVD). A gas containing Carbon, often methane, is ionised and the non-carbon atoms removed. This removal of the non-carbon atoms, in case of methane Hydrogen, is done by free radicals, i.e. unbound atoms such as atomic Hydrogen. As Hydrogen is normally only found in a bound state, a plasma is created. The free Carbon atoms settle on a substrate. They can move on its surface as the substrate is heated. At a seeding spot the Carbon atoms will either build graphite or diamond crystals. At low pressure and high temperature graphite $sp^2$ bonds are energetically favoured over the diamond $sp^3$ bonds. However, the free Hydrogen atoms will remove some Carbon from the substrate. The rate of this process depends on the type of bond. Graphite bound Carbon atoms are removed approximately a hundred times more frequent than diamond. This means that virtually no graphite is left on the substrate.
Crucial parts of this process are the plasma generation and the mixture of a Carbon containing gas and Hydrogen in an Argon atmosphere. Most commercial suppliers for CVD diamonds use microwaves to generate the plasma. A sketch of such a CVD unit is presented in Figure 3.1.

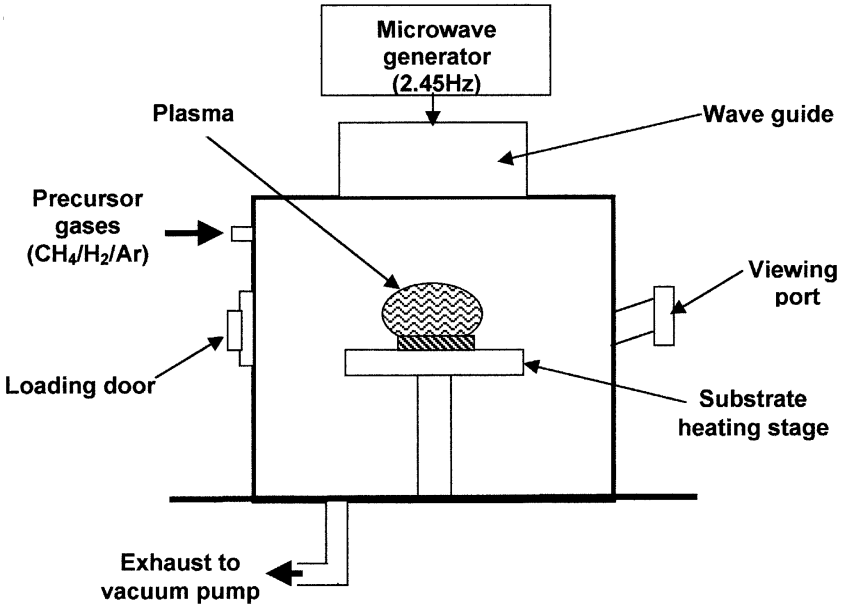


***Figure 3.1.:*** Schematic of an apparatus for producing CVD diamonds. The plasma is generated using a microwave generator [9].

Another important aspect is the type of the substrate. If a non diamond substrate is used, i.e. silicon, the diamond growth will start in several spots distributed over the substrate surface. This forms separate singlecrystalline grains, with slightly different orientations. When they grow further and eventually merge, grain boundaries will arise from these different orientations. As growth in certain directions is favoured, the number of grains will decrease with the thickness of the diamond. Such diamonds are called polycrystalline (pCVD) diamonds. To improve the quality of the diamond, i.e. reduce the number of grains, the diamond is polished from both sides. But as mentioned above the number of grains reduces in direction of the growth side. So this side is only polished to receive a flat surface. From the substrate side a large chunk, typically a few hundred micrometers, is removed.

To produce a singlecrystalline (scCVD) diamond a diamond substrate is needed. This substrate has to be a singlecrystal itself. As the Carbon atoms will bond to an already evenly oriented diamond structure all seed spots have the same orientation. This prevents the development of grain boundaries when the seed spots merge. After production the diamond is cut from the substrate with a laser.

The need for a singlecrystalline substrate to produce scCVD diamonds significantly limits the size of the produced diamonds to approximately 1 $cm^2$ compared to full wafer sized pCVD diamonds. However, this value has increased in the last years and probably will improve even further.

| property | diamond | silicon |
|---|---|---|
| band gap [eV] | 5.47 | 1.12 |
| breakdown field [V/cm] | $10^7$ | $3 \cdot 10^5$ |
| resistivity [$\Omega$ cm] | $> 10^{15}$ | $2.3 \cdot 10^5$ |
| intrinsic carrier density [cm$^{-3}$] | $< 10^3$ | $1.5 \cdot 10^5$ |
| mass density [g cm$^{-3}$] | 3.52 | 2.33 |
| atomic charge | 6 | 14 |
| dielectric constant | 5.7 | 11.9 |
| displacement energy [eV/atom] | 43 | 13 - 20 |
| energy to create e-h pair [eV] | 13 | 3.6 |
| radiation length [cm] | 12.2 | 9.4 |
| avg. signal created/$\mu$m [e] | 36 | 89 |
| avg. signal created/0.1% rad. length $X_0$ [e] | 4400 | 8400 |

***Table 3.1.:*** Comparison of properties of diamond and silicon [5].

## 3.2. Fundamental properties of diamond

So far, the most commonly used sensor material in high energy physics is silicon. But with the increasing requirements for new detectors, silicon may reach its limits. Especially its radiation hardness is considered critical for applications like the sLHC. Diamond on the other hand has proven to be very radiation hard [10]. Despite being an electrical insulator it can be used for solid state detectors. A comparison of the properties of diamond and silicon is summarised in Table 3.1.

Diamond, being an insulator, has a very high resistivity. This significantly decreases the leakage current compared to Silicon. As the shot noise is proportional to the square root of the leakage current it is very low in diamond sensors.

The band gap in diamond is roughly five times larger than in silicon. This increases the energy needed to create an electron-hole pair in diamond to 13 eV compared to 3.6 eV in silicon. So the signals in diamond are smaller for the same deposited energy. But the larger band gap is also a strength of diamond, as it decreases thermal noise significantly. It is possible to run diamond detectors with little to no cooling without encountering problems associated with noise. Also due to the high thermal conductivity cooling is very effective.

Due to its lower dielectric constant the capacitance of diamond is lower than for silicon. So the capacitive load on the read-out electronics and thus the noise level is lower as well. Another positive aspect of diamond is the high mobility and saturation velocity of electrons and holes. Thus the response time of the detector can be very low. This

is important for environments with high particle flux such as for the ATLAS upgrade project of a new innermost layer of the Pixel detector, IBL [11], or sLHC [12]. Due to the high breakdown field of $10^7$ V/cm of diamond it is possible to apply high voltages to such a sensor. At high electric fields the saturation velocities of the charge carriers can be reached and the overall charge collection benefits from this (see Equation 3.1).
The roughly 40% longer radiation length of diamond compared to silicon means that less energy per distance is deposited in diamond. This and the larger band gap result in a much smaller signal from a particle in diamond for equally thick sensors. But in combination with only minimal or no cooling for the sensor itself the material budget of a diamond detector can be very low.
However, a major disadvantage is charge trapping on e.g. grain boundaries. When the charges are trapped they can no more contribute to the signal. Thus trapping decreases the signal. Using single crystalline diamonds and other improvements can increase the mean free path of charge carriers and thus limit charge loss.
The energy needed to remove an atom permanently from its place in the crystal lattice - the displacement energy - is at least two times higher in diamond than in silicon. This contributes to the radiation hardness of diamond as damages of this type will occur less often. As this is the main process inflicting damage in the sensor material of tracking detectors, it is a major advantage of diamond over silicon.
Thus diamond will probably not fully replace silicon tracking detectors. But the low material budget of a full detector, its radiation hardness and low noise level are good reasons to build at least the inner most layer of a tracking detector for a hadron collider of diamond sensors.

## 3.3. Charge collection distance

One of the main problems of diamond sensors is charge loss through trapping. This means that charges induced by a particle do not propagate through the whole sensor to the electrodes but are trapped on the way. However, due to Ramo's theorem (see Equation 2.2) a current is still induced on the electrodes. As stated before, to measure the full charge, the carriers have to reach the electrodes. In case they are trapped before, only a fraction $q_m$ of the full charge $q_0$ is measured. The ratio of these two values is an intrinsic parameter for each diamond and has to be known to interpret the signals correctly. A derived figure of merit is the charge collection distance (CCD) which equals

the mean distance electrons and holes drift apart before being trapped. It is defined as [5]

$$\mathrm{CCD} = (\mu_e \tau_e + \mu_h \tau_h) E \ . \tag{3.1}$$

$\mu_{e,h}$ denotes the mobility of electrons and holes, $\tau_{e,h}$ their lifetime and $E$ the applied electric field. Assuming that the CCD does not exceed the thickness $d$ of the sensor, another equivalent definition is possible:

$$\mathrm{CCD} = d \, \frac{q_m}{q_0} \ . \tag{3.2}$$

This is a handy definition to measure the CCD, if the induced charge $q_0$ is known.
The aim for the CCD is to exceed the thickness of the sensor as only in this case the full charge can be measured. This is important as only few charges, compared to silicon, are produced in the beginning. So a further decrease is very disadvantageous.
Trapping of charges is often associated to grain boundaries so the CCD of an scCVD diamond should be longer than that of a pCVD diamond. In the past only scCVD diamonds could have CCDs which exceed the thickness of the sample. This is now also possible for pCVD samples but these have to be of high quality. To improve the CCD several methods are available. A higher bias voltage increases the charge carrier velocity and thus the CCD up to the saturation of the velocity.
Irradiation with a strong source can also increase the CCD. This so called pumping fills the charge traps and thus reduces the trapping of signal charges. It is naturally reversed over time. However, this detrapping is very slow for most traps and takes at least several days. Heating the sample and exposure to UV light also reverse immediately the pumping. So careful handling of a pumped sensor is necessary.
Compared to silicon, diamond is very radiation hard, up to sLHC doses. This is due to the displacement energy, which is at least twice as high as for silicon. Also for equally thick samples the deposited energy is lower, as the radiation length is about 30% longer compared to silicon. This is an advantage as it reduces the material budget. Due to the longer radiation length multiple scattering occurs less often.
For measurements of the CCD the diamond sample is irradiated by a radioactive source. The resulting spectrum is then compared to the expected. If it is shifted to lower charges the CCD does not exceed the sensor thickness. Experimental results show that for scCVD diamonds not only the CCD is longer but also the energy resolution is better than for pCVD diamonds [5]. This can be attributed to the absence of grain boundaries in scCVD diamonds as charges are easily trapped at these points. Trapping is a statistical process and thus more trapping decreases the resolution.

## 3.4. C-V measurement

As the leakage current and thus the shot noise of a detector made of an intrinsic semiconductor, e.g. silicon, would be too high to detect any particles, a p-n-junction is used. This junction consists of two differently doped semiconductors. The n-type semiconductor is doped with donors which means that the doped atoms have five valence electrons. The additional electron is only weakly bound and has an energy level close to the conduction band. For a p-type semiconductor it is the other way round. The doped atoms are missing an electron and thus introduce holes with an energy level close to the valence band. The electrons and holes recombine near the interface. This creates a space charge region called depletion zone. It is typically expanded through the whole sensor via an external reverse bias voltage.
Charges in this depleted region are collected and thus it is important to know what bias voltage has to be applied to completely deplete the sensor. The width $W$ of the depleted region can be calculated via [13]

$$W = \sqrt{\frac{2\varepsilon_0\varepsilon_r(N_A + N_D)}{eN_AN_D}(V_{bi} - V_{ex})} \; . \tag{3.3}$$

$\varepsilon_0$ and $\varepsilon_r$ are the vacuum and relative permittivity, respectively. $e$ is the elementary charge. $N_A$ and $N_D$ are the concentration of acceptors and donors, respectively. $V_{bi}$ is the potential caused by the depleted region in thermal equilibrium and $V_{ex}$ is the external bias voltage. For the case of reverse biasing it is $V_{ex} < 0$.
Typically one type is much heavier doped than the other. The advantage is that the depleted region propagates nearly exclusively into the weaker doped side. Assuming a heavily doped p-type and a weakly doped n-type Equation 3.3 simplifies to

$$W = \sqrt{\frac{2\varepsilon_0\varepsilon_r}{eN_D}(V_{bi} - V_{ex})} \; . \tag{3.4}$$

To calculate the width of the depletion region the doping concentration of the weakly doped material has to be known. This concentration can be derived from the variation of the capacitance with respect to the applied bias voltage. The Ansatz for this calculation is

$$\frac{\mathrm{d}C}{\mathrm{d}V_{ex}} = \frac{\mathrm{d}C/\mathrm{d}W}{\mathrm{d}V_{ex}/\mathrm{d}W} \; . \tag{3.5}$$

The capacitance $C$ of a fully depleted p-n-junction can be approximated by a parallel plate capacitor. Its capacitance is given by

$$C = \varepsilon_0 \varepsilon_r \frac{A}{W} \, . \tag{3.6}$$

$A$ denotes the area of the electrodes. The derivative of the external voltage with respect to the depletion width can be calculated via

$$\frac{\mathrm{d}V_{ex}}{\mathrm{d}W} = -\frac{\mathrm{d}(V_{bi} - V_{ex})}{\mathrm{d}W} + \frac{\mathrm{d}V_{bi}}{\mathrm{d}W} \, . \tag{3.7}$$

The variation of the internal bias voltage $V_{bi}$ with respect to the depletion width is very small and can be neglected. So combining Equation 3.7 with Equation 3.4 yields

$$\frac{\mathrm{d}V_{ex}}{\mathrm{d}W} = -W \frac{eN_D}{\varepsilon_0 \varepsilon_r} \, . \tag{3.8}$$

Using this result and Equation 3.6, the derivative in Equation 3.5 can be solved to [14]

$$\begin{aligned} \frac{\mathrm{d}C}{\mathrm{d}V_{ex}} &= \frac{\varepsilon_0 \varepsilon_r A / W^2}{W e N_D / (\varepsilon_0 \varepsilon_r)} \\ &= \frac{(\varepsilon_0 \varepsilon_r)^2 A}{W^3 e N_D} \\ &= \frac{C^3}{\varepsilon_0 \varepsilon_r A^2 e N_D} \\ \Rightarrow N_D &= \frac{C^3}{\varepsilon_0 \varepsilon_r A^2 e} \cdot \left( \frac{\mathrm{d}C}{\mathrm{d}V_{ex}} \right)^{-1} \, . \end{aligned} \tag{3.9}$$

The last equation gives information about the overall doping concentration at a specific depletion depth $W$. For a full profile of the concentration it has to be measured at different voltages. These voltages can be transfered into the depletion depth.
Unirradiated diamond sensors are neither doped nor have intrinsic uncompensated charge centers. The expected result for $N_D$ or $N_A$ is zero. This means that the change of capacitance with respect to the bias voltage has to be infinite according to Equation 3.9. This shows that the model does not describe diamond well. The assumption that the depletion depth depends on the bias voltage is not valid for a perfect diamond crystal which is free of intrinsic charges. For a diamond the whole sensor is free of space charge even if no external voltage is applied. So what is expected in this case is that the capacitance does not change at all with respect to the applied voltage.
But through a high irradiation dose traps are induced in the diamond. If these traps are

ionised they act like doping atoms. The behaviour of the trapping centers with respect to the bias voltage depends on the energy level of the respective trap. Different traps can be neutralised or ionised, depending on their distance from the valence and conduction band. Therefore the occurance of traps is noticeable by a change of capacitance with respect to the bias voltage, although it should be very small.
For semiconductor sensors it is known that high irradiation doses change the effective doping concentration and even invert the type of doping [15]. So the C-V measurement may be a method to quantify the damage of the irradiation to the diamond. However, as the diamond has no p-n-junction and thus no clear majority charge carrier this description is not perfect.

# 4. Bulk segmentation

## 4.1. Motivation for new types of electrodes

The efficiency of a diamond sensor depends on the charge collection distance (CCD) and thus also on the distance between the electrodes. As mentioned in Chapter 3.3 the CCD for good samples can be larger than their thickness. But due to the statistical behaviour of trapping this does not yield an efficiency of 100% as the CCD is only the mean distance a charge carrier travels before being trapped. The aim for diamond sensor production is to exceed the distance between the electrodes with the CCD as much as possible. This can be achieved by using diamonds with larger CCDs or by reducing the distance between the electrodes.

Diamonds with larger CCD are generally scCVD diamonds due to the absence of grain boundaries. Some good pCVDs have also large CCDs but these are expensive and have a slow production rate. So both cases would significantly increase the costs for a diamond detector compared to using cheap pCVD diamonds. Additionally, the production of scCVD diamonds is much slower and more complicated. Polycrystalline diamond can be grown in full wafer size whereas areas of only about 1 $cm^2$ are achieved with singlecrystalline diamond.

Another reason to not just rely only on the higher CCD of scCVD diamonds is the decrease of CCD in both types of diamond with increasing radiation dose. An experimental result is illustrated in Figure 4.1. It can be concluded that the CCD decreases exponentionally with respect to the radiation dose for both types. Moreover, they even have the same damage constant. This is shown by a shift of the scCVD data to lower fluencies so that it fits to the damage curve of the pCVD samples for negative fluencies. Thus scCVD diamonds have a higher initial CCD but after irradiation of - in this example - $3.8 \cdot 10^{15}$ protons/$cm^2$ they have the same CCD as the unirradiated pCVD sample. This hints that processes of the damage of the bulk from irradiation is for both types the same. Especially scCVD diamond is not radiation harder than pCVD diamond. So scCVD diamonds have a satisfying CCD when unirradiated but at high doses they suffer under the same low values as pCVD diamond.

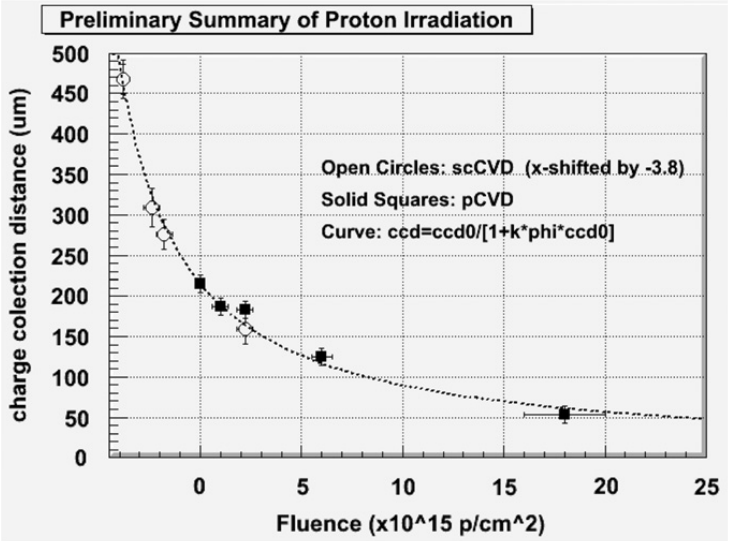


***Figure 4.1.:*** Measured CCD before and after irradiation with 24 GeV protons for scCVD (open circles) and pCVD (solid squares) diamond. For both types the CCD at zero fluence is normalised to 220 µm. The data for scCVD diamond is shifted to the left to match the damage curve of the pCVD diamond. This shows that both types have the same damage constant [16].

The more promising approach to have full charge collection efficiency even at a high radiation dose is to reduce the space between the electrodes. Most modern hybrid tracking detectors use a planar electrode design, e.g. the ATLAS Pixel Detector [17]. This means that reducing the space between electrodes results in thinner sensor material, which is often unfavourable as the deposited charge and thus the signal decreases and the sensor is more vulnerable to mechanical stress. An alternative to this design are 3D-sensors [18]. In this case the electrodes are not on the surface of the sensor material but penetrated inside the bulk. This concept is illustrated in Figure 4.2. It has several general advantages compared to planar sensors like lower depletion voltage for semiconductors and faster charge collection while still retaining the full signal. In diamond sensors the main advantage is the decreased distance between the electrodes, which reduces the influence of trapping.
Two general designs of 3D sensors are available. In the first design the electrodes completely penetrate the sensor. This has the advantage that both electrodetypes can be contacted from the same side. On the other hand this can cause problems if the density of the electrodes is very high as in this case it is more difficult to just connect one type of electrode with each other. The major disadvantage of this design is also a general problem of 3D sensors. If a particle passes perpendicular through the sensor it may deposit all its energy in one of the electrodes. As these charges cannot be collected, the efficiency drops at the electrodes. To tackle this in another design the electrodes are implemented from the

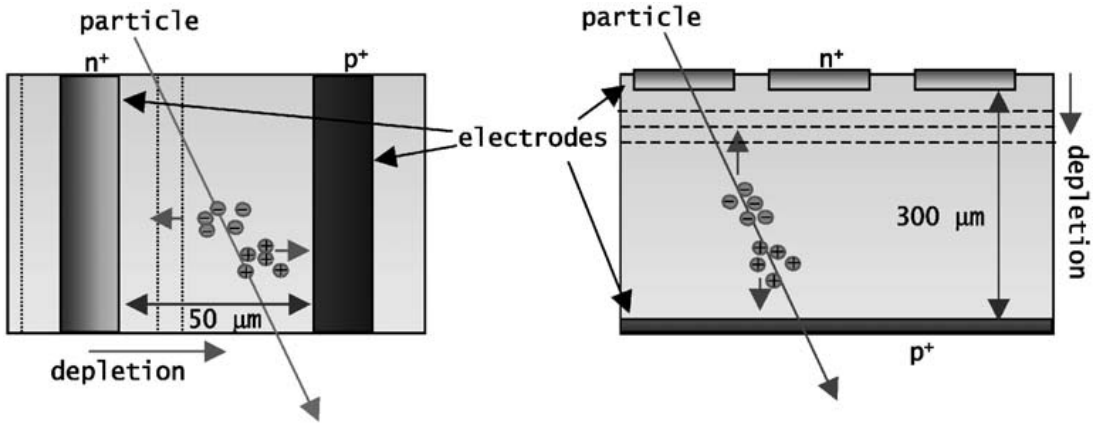


***Figure 4.2.:*** Sensor with 3D (left) and planar (right) electrodes. In both cases the same amount of charge is deposited by the incoming particle as it has to pass the full sensor thickness. But for the 3D electrodes these charges are generated much closer to the electrodes. As the spacing between them is lower, for semiconductors the depletion voltage decreases [19].

two sides of the sensor and maintain a gap to the other end of the sensor approximately equal to the spacing of the electrodes. Now even if a particle passes through an electrode it deposits some amount of charge in the sensor bulk. Furthermore the whole modules can be mounted not perpendicularly but slightly tilted with respect to the interaction point. This reduces the probability of such an event.
It is also possible to increase the resolution of detectors with 3D-sensors, as the distance in silicon between the electrodes can be as low as 50 µm in all directions [20]. As this forces the read out electronics to be at this size, too, current testing with 3D-sensors is done by connecting several electrodes of the same type on the surface. Thus the current ATLAS Pixel read out chip, the FE-I3, can be used [21].

## 4.2. Graphitisation of diamond

For operation with planar electrodes a diamond sample can be metallised with e.g. pixellated electrodes. These metal contacts can easily be stripped off and remade as the diamond is not damaged during this process. This is not as simple for 3D electrodes as they are deposited inside the diamond bulk. Several techniques to drill holes for the electrodes into Silicon are available [22]. But most of these, e.g. etching, will not work with diamond due to its unique chemical characteristics.
To build an electrode in diamond it is not needed to drill an actual hole in the material. As diamond consists of Carbon, a conversion of the diamond $sp^3$ lattice to graphite $sp^2$

lattice is enough for a conducting electrode. To convert the bonds several methods are available but not all capable of producing long graphite pillars in the diamond bulk.
Using high pressure up to 2 GPa and heating the diamond to 1300 K causes a controlled conversion of around 30% of the diamond bonds [23, 24]. So far, this only works with thin diamonds of 30 - 40 µm. For thicker diamonds much higher pressures are needed. Furthermore the process takes 30 minutes per spot. These points rule out this method for the fabrication of 3D sensor electrodes.
Simply heating the whole diamond also works but this graphitisation process cannot really be controlled [25]. The conversion usually starts at impurities which have to be created carefully before heating the sample.
But heating single atoms of the diamond is also possible by irradiating it with ions. For nano sized diamonds full graphitisation can be achieved [26]. Computer simulations show that a minimum transfered energy for the heated atoms is needed for the diamond to convert to graphite [27, 28]. These thresholds differ in the two publications from 416 eV resulting in a fraction of 62% $sp^2$ bonds found by Saada *et al.* and 2.58 eV causing $(34 \pm 5)\%$ $sp^2$ bonds found by Sorkin *et al.*. The difference can be explained with the fact that in the first publication twelve atoms are heated to this energy but one at a time whereas in the second four layers with a total of 16 atoms are heated at once. The minimum percentage of graphit bound Carbon atoms for a conducting layer is determined by Sorkin *et al.* to be 45%.
These results clearly show the limitation of this process. It is not enough to excite single Carbon atoms to produce graphite bonds. Instead several at close range have to be hit by the ions. Heavy ions can transfer these energies in single collisions, but due to their high stopping power they do not penetrate deeply into the diamond. Even assuming a typical proton from a tandem accelerator with 6 MeV penetrates the diamond only approximately 200 µm deep. This means that the diamond has to be flipped and irradiated from both sides which can cause problems. But such protons may not pass enough energy per collision to cause $sp^2$ bonds. Thus irradiation with ions is not really suitable for the formation of graphite pillars in the diamond bulk. However, the transformation works at the surface using heavy ions [29, 30, 31].
All methods described above heat the Carbon atoms in some way. Another approach is to excite the electrons from the valence into the conduction band with a femtosecond laser [32, 33, 34]. Single very hot, i.e. high energetic, electrons can cause an avalanche ionisation. If the density of the excited electrons is large enough, a phase transition from diamond to graphite is induced. Although the band gap of diamond of 5.47 eV is too large to excite an electron with a single photon from an 800 nm laser other effects occur with

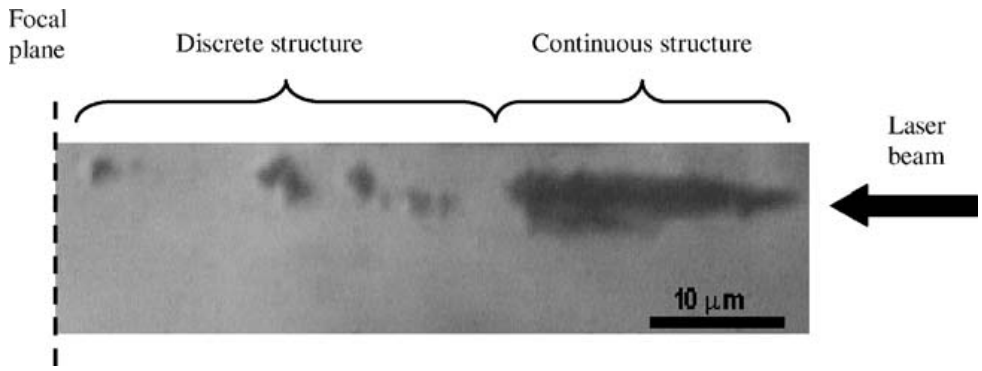


***Figure 4.3.:*** Image of graphite impurities in diamond produced by multiple shots using a 120 fs laser. The separation into two types of structures is visible [32].

femtosecond lasers. These effects are nonlinear photoionisation and multiphoton ionisation and are caused by the high electric field of the laser. Depending on the frequency and intensity of the laser one or the other effect dominates. For an 800 nm laser both effects are shown to contribute equally [32].

In Figure 4.3 the graphitisation of diamond using an 800 nm laser with pulses of 120 fs and a total deposited energy of 320 nJ can be seen. The damaged region lies upstream of the focal plane. It can be seen that the transformation is separated into two regions. One with discrete structures and one with continuous growth. This shows that the fluence $F$ has significant impact on the structure of the graphitisation. At the boarder of these two regions the fluence is calculated to be $F_{th}^1 = (1.2 \pm 0.2)\ \frac{\mathrm{J}}{\mathrm{cm}^2}$. A fluence higher than this threshold yields a discrete structure, lower fluence results in a continuous graphitisation. If the fluence is high ($F > F_{th}^1$) several distinct graphitised spots are created. These grow so fast that the one furthest away from the focal plane, i.e. the first one in the beam, absorbs the beam. Thus the other seeds stop growing. For a lower fluence the spots grow significantly slower so that a continuous structure is generated. This structure will grow until the fluence drops below a threshold of $F_{th}^2 = (0.35 \pm 0.05)\ \frac{\mathrm{J}}{\mathrm{cm}^2}$. Below this threshold no growth is observed at all. If the fluence is always lower than $F_{th}^1$ an exclusively continuous growth is realised. As the structure stops growing when $F < F_{th}^2$, the focal plane has to be moved through the thickness of the sample to continue the growth of the graphite pillars.

The continuous region is very interesting for diamond sensors as this may provide a technique to grow graphite electrodes in the sensor bulk. Important for this are the length and diameter of such pillars. The length of the continuous growth region can be extended by just moving the sample away from the focal plane of the laser. Depending on the speed of this movement the diameter can also be controlled as illustrated in Figure 4.4. A speed

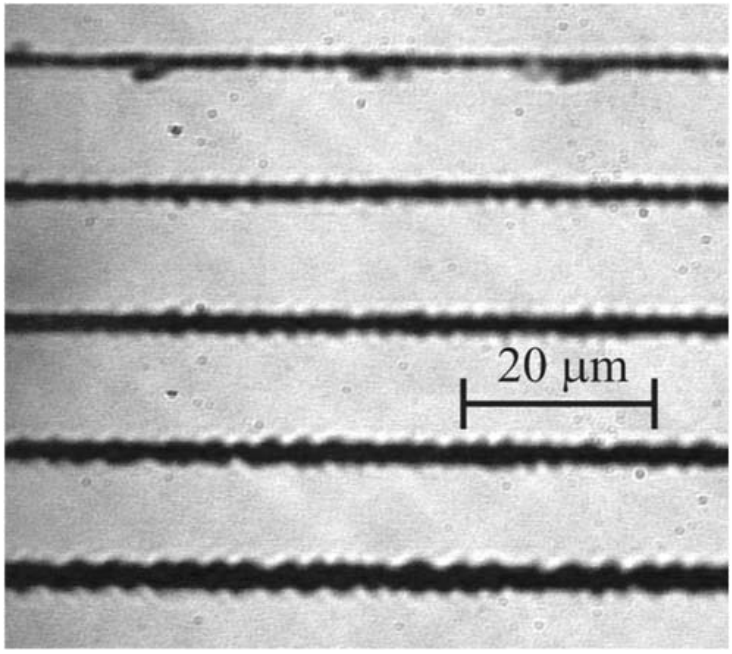


***Figure 4.4.:*** Graphite tubes in diamond produced with an 800 nm laser which is pulsed with 140 fs at a repetition rate of 1 kHz. From top to bottom the speed of the moving sample was 1 $\frac{\mu m}{s}$, 3 $\frac{\mu m}{s}$, 5 $\frac{\mu m}{s}$, 10 $\frac{\mu m}{s}$ and 30 $\frac{\mu m}{s}$ [33].

of 30 $\frac{\mu m}{s}$ results in a diameter of approximately 3.5 µm. This diameter is small enough for a sensor electrode as the spacing between them would be around 50 µm. This value can be decreased down to a diameter of 1 µm [34]. The maximum length of such a tube was 680 µm which is more than the expected thickness of a diamond sensor. In this case the length was only limited by the thickness of the sample.

As one sensor needs at least a few ten thousands of those electrodes, the time needed for fabrication is also very important. Considering a growth rate of 30 $\frac{\mu m}{s}$ and a sensor thickness of about 400 µm one electrode takes approximately 14 s to produce. As the positioning can be automated moving the sensor to the next electrode is fast. Using more than one laser or splitting the beam of a high power laser can further decrease the production time.

From these facts it can be concluded that using a femtosecond laser may be a very powerful way to fabricate 3D diamond sensors. However, there are a few restrictions. The pulses of the laser have to be in the range of femtoseconds as e.g. 300 ps pulses produce highly frayed out structures [32]. Also the quoted thresholds for the graphitisation may vary between samples especially comparing scCVD and pCVD diamond. As the later one has grain boundaries which can reflect parts of the laser beam, this may increase the fluence locally and cause a phase transformation below the nominal threshold.

The transformation also does not depend only on the fluence but also slightly on the

number of laser pulses. This dependence may be due to stable nano sized defects caused at lower fluence, which only grow slowly with each pulse.
Cracking of the diamond due to the graphite tubes seems not to be a problem. Although diamond is more than twice as dense as graphite, layers with graphite pillars of 1 µm diameter with a gap of only 1 µm have been produced without damaging the diamond bulk [34]. Small cracks directly at the electrodes might also act as charge traps.

# 5. C-V measurement

## 5.1. Experimental setup

An Agilent B1505A Semiconductor Device Analyzer is used to measure the capacitance of the diamond samples. The diamond is put in a metal box which acts as a Faraday cage to reduce electro-magnetic pick-up and protects the sample from light. A picture of the whole setup can be seen in Figure 5.1.

### 5.1.1. The diamond fixture

Figure 5.2 shows a picture of the open fixture used to hold the diamond sample. The upper electrode is connected to the diamond via a spring. At the end the spring has a small bump such that a contact to the diamond electrode is established. Below the spring is a copper plate. In this plate a round rivet is embedded to contact the lower electrode. The contacts are mounted on a plastic block to insulate them from the metal box. As the amount of measured charges is very small a good shielding of the whole setup is needed to reduce the electro-magnetic pick-up and thus the overall noise level of the system. Thus the metal box acts as a Faraday cage but also protects the diamond from light sources. This is important as UV-light unpumps the diamond.

### 5.1.2. The B1505A Semiconductor Device Analyzer

Unlike e.g. current or voltage the capacitance of a device in an electric circuit cannot be measured directly. But from the impedance $Z$ of the device the capacitance $C$ can be calculated using

$$\begin{aligned} Z &= \frac{1}{2\pi f C} \\ \Leftrightarrow C &= \frac{1}{2\pi f Z}\,. \end{aligned} \tag{5.1}$$

The frequency $f$ has to be chosen, so that it affects the measurement as little as possible. For high frequencies the inductance of the cables can become dominant, for low

***Figure 5.1.:*** Photograph of the B1505A. On top of it lies the metal box including the fixture for the diamonds and a bias tee to connect it with the B1505A.

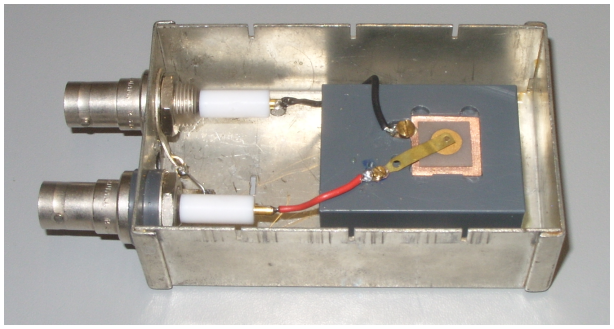

***Figure 5.2.:*** Photograph of the open fixture with a diamond sample inserted. The upper electrode of the diamond is connected via a spring, the lower via a round rivet.

frequencies the measured value of the unknown impedance may be too high for an accurate measurement. Therefore too high or too low frequencies might change the value for the capacitance. Thus to measure the capacitance one needs to measure the impedance at a specific frequency.

The B1505A can measure the impedance of a DUT up to a bias voltage of $\pm 3$ kV and with frequencies ranging from 1 kHz to 5 MHz. To determine the impedance it uses an auto balancing bridge method.

Figure 5.3 shows a scheme of such a bridge measurement. It consists of three known impedances $Z_i$ of which at least one can be varied. The impedances are adjusted such that no current flows through $D$, i.e. balancing the bridge. If this is the case, the ratio of

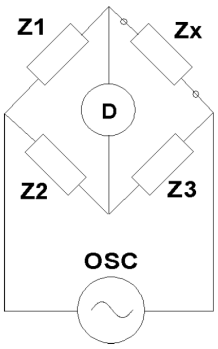


***Figure 5.3.:*** Measurement of impedance $Z_x$ using the bridge method. The three known impedances $Z_i$ are adjusted, such that no current flows in the detector $D$ [35].

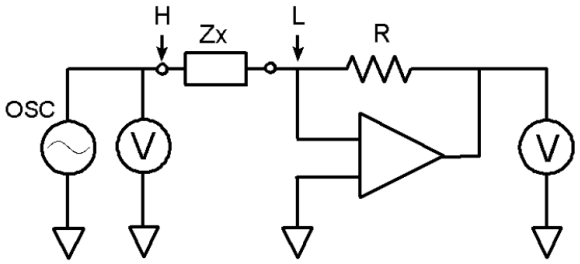


***Figure 5.4.:*** Simplified sketch of the measurement of impedance $Z_x$ using the auto balancing bridge method. A virtual ground is generated at point $L$, thus the same current flows through the unknown impedance $Z_x$ and the known resistor $R$. The impedance is calculated from the potential over the resistor $R$ and over $Z_x$ [35].

the impedances $Z_1$ and $Z_2$ equals those of $Z_x$ and $Z_3$.

$$\begin{aligned} \frac{Z_1}{Z_2} &= \frac{Z_x}{Z_3} \\ \Leftrightarrow Z_x &= Z_3 \cdot \frac{Z_1}{Z_2} \end{aligned}$$

The auto balancing bridge method also uses the current to determine the impedance, but unlike the bridge method the current through the unknown impedance is mirrored in a known resistor and measured directly. A sketch of this method is given in Figure 5.4. To have the same current in the impedance and the resistor, point $L$ in Figure 5.4 is kept fixed at ground potential. To achieve this a detector at this point controls the not ideal amplifier so that no potential is detected. From the measurement of the voltage over the

impedance $U_x$ and the voltage $U_R$ over the resistor $R$ the impedance $Z_x$ can be calculated.

$$\begin{aligned} Z_x &= R \cdot \frac{U_x}{U_R} \\ \overset{5.1}{\Rightarrow} C_x &= \frac{1}{2\pi f} \cdot \frac{U_R}{R U_x} \end{aligned}$$

The model described above is simplified as for a measurement of the impedance the vector components of the voltage needs to be known, i.e. active and reactive voltage. Thus the amplifier and the measurement of the two voltages have to be expanded with components to measure the vector components of the voltage.
As the expected capacitance of the diamond is very low, an important thing is to compensate the stray capacities and inductances. These result from cables and the setup in general. For low values of the unknown capacitance the stray capacities can have a significant influence on the measured value. The correction is done via the short and open compensation. For both compensation measurements everything is connected as for a measurement but the diamond is removed from the fixture. During the short compensation the electrodes are connected directly to each other, i.e. shorting them. This theoretically leads to zero impedance. The measured difference to this value can be attributed to stray capacities and is subtracted from the measurements.
The open compensation is just the other way round. The electrodes have no contact and thus the impedance should be infinite. Again, if a value for the capacitance can be measured, this is due to stray capacities and can be compensated.

### 5.1.3. Diamond samples

#### Sample 1: Highly irradiated diamond

This sample is a pCVD diamond which was highly irradiated. Such a high dose alters the appearance of the diamond as it has lost its optical quality and is opaque. A picture of it is shown in Figure 5.5 (a,b). Because this diamond sample is very old it has a smaller grain size and thus more grain boundaries than newer pCVD samples as these profit from improved production processes. The seed and growth side can be clearly distinguished which shows that the diamond was not polished. Its surface is quadratic and measures approximately 1 $cm^2$. It has a thickness of $(400 \pm 10)$ µm. The electrodes are made of gold and have a circular shape and a diameter of $(6.079 \pm 0.001)$ mm.

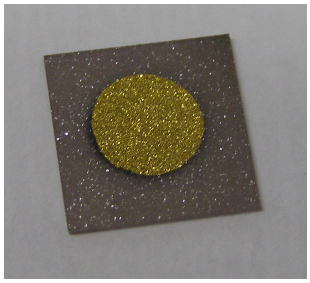

(a) Diamond sample 1, growth side.

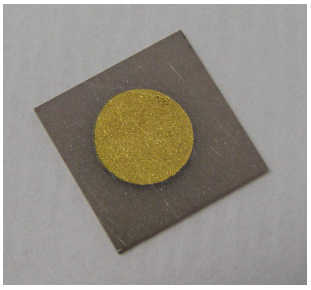

(b) Diamond sample 1, substrate side.

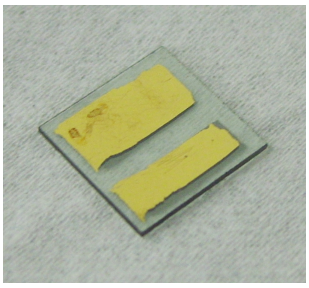

(c) Diamond sample 2.

***Figure 5.5.:*** Pictures of the diamond samples.

**Sample 2: Irradiated diamond**

This sample was irradiated with $3 \cdot 10^{15}$ 25 MeV protons per square centimeter. Nevertheless this pCVD diamond has still optical quality as can be seen in Figure 5.5 (c). The electrodes are separated on both sides in two parts. For measurements only the bigger electrode was used. Also the electrodes on both sides are not made from the same material. The side used for collecting the charges and applying the high voltage is made of gold and on the other side of TiW. The diamond has a thickness of $(520 \pm 5)$ µm.

**Sample 3: Unirradiated diamond**

This diamond sample was never exposed to huge amounts of irradiation. The physical size of this pCVD diamond is rather small with the gold electrodes having an area of $(0.133 \pm 0.005)$ cm$^2$ each. It has a thickness of $(507 \pm 5)$ µm and is of optical quality.

## 5.2. Experimental results

### 5.2.1. Calibration

To determine the capacitance a periodic voltage pulse has to be applied to the device under test (DUT), i.e. the diamond sample. It is important to know if the capacitance varies with respect to this frequency and its amplitude. Thus at a bias voltage of 0 V it is measured for different frequencies. For better statistics, the measurement is repeated 1001 times with an interval of 500 ms for each frequency. As the program of the B1505A does not allow repeated measurements at the same bias voltage, the voltage is swept from 0 V to 1 mV with a nominal interval of 1 µV. However, this sweep can be considered as a measurement at fixed bias voltage as Figure 5.6 shows in which all measured bias

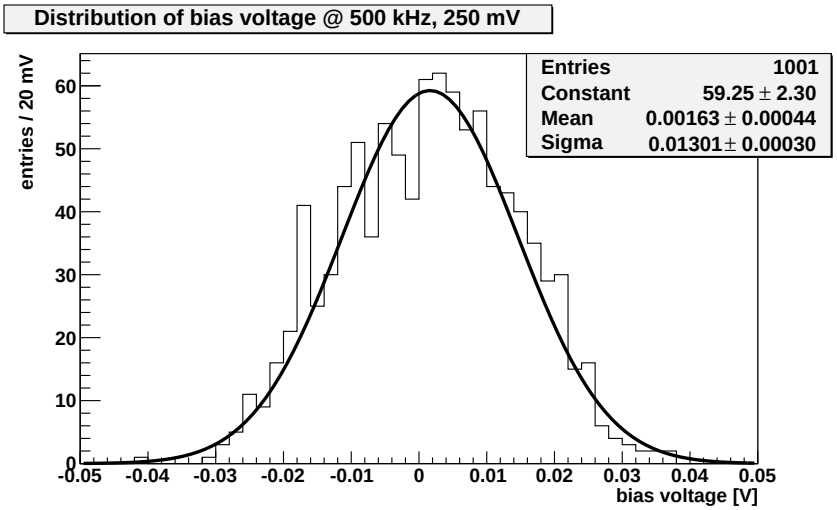


***Figure 5.6.:*** Distribution of the measured bias voltage during one capacitance measurement at 0 V. The uncertainty of the voltage supply exceeds the uncertainty induced by a voltage sweep from 0 V to 1 mV.

| frequency [kHz] | capacitance [pF] | statistical error [pF] | systematic error [pF] |
|---|---|---|---|
| 1 | 3.691 | 0.004 | 0.244 |
| 100 | 3.941 | $4 \cdot 10^{-4}$ | 0.008 |
| 500 | 3.940 | $5 \cdot 10^{-4}$ | 0.007 |
| 1000 | 3.948 | $3 \cdot 10^{-4}$ | 0.007 |
| 5000 | 4.204 | $5 \cdot 10^{-4}$ | 0.021 |

***Table 5.1.:*** Mean values of capacitance for 1001 measurements at a bias voltage of 0 V and an oscillator level of 250 mV for different frequencies.

voltages during one sweep are histogrammed. The distribution has a Gaussian shape and the mean value is $1.6 \pm 0.4$ mV. The shape indicates that the deviation of the bias voltage is not due to the sweep but rather to the intrinsic uncertainty of the high voltage supply. This explains why the mean value is higher than the nominal start and end voltage of the voltage sweep. The sigma of $13.0 \pm 0.3$ mV is more than ten times higher than the amplitude of the voltage sweep. So it is fair to assume that the influence of the sweep on the measurement is negligible.

An example of such a measurement at constant bias voltage is given in Figure 5.7. This and all following measurements for calibration are performed using the highly irradiated diamond sample 1. As the bias voltage is set to 0 V the capacitance is stable in time. The mean capacitance is calculated by histogramming all measured data values and fitting a Gaussian distribution. Its sigma gives the statistical error for the mean value.

The results for different frequencies are given in Table 5.1. Plots for the individual mea-

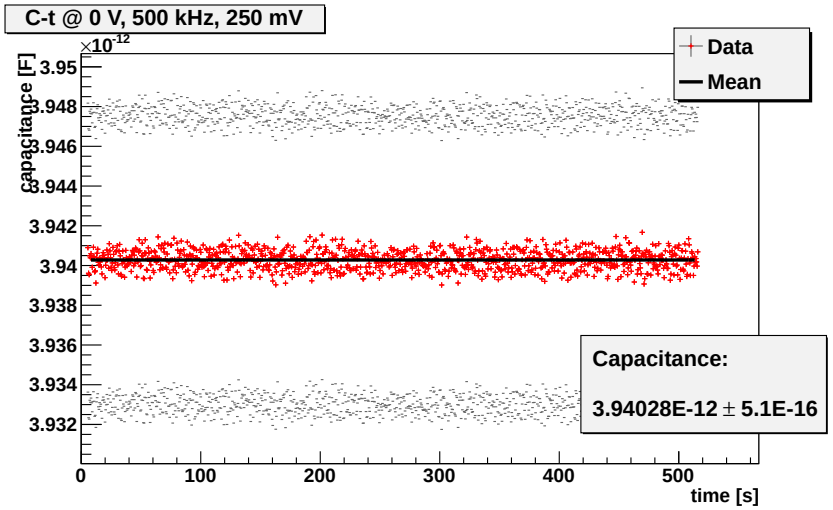


***Figure 5.7.:*** Measurement of capacitance at a constant bias voltage of 0 V and a frequency of 500 kHz. The error for each data point indicate the systematic uncertainty. The error on the capacitance is the statistical error.

| amplitude [mV] | capacitance [pF] | statistical error [pF] | systematic error [pF] |
|---|---|---|---|
| 32 | 3.940 | 0.004 | 0.009 |
| 64 | 3.940 | 0.002 | 0.008 |
| 125 | 3.940 | 0.001 | 0.008 |
| 250 | 3.940 | $5 \cdot 10^{-4}$ | 0.007 |

***Table 5.2.:*** Mean values of capacitance for 1001 measurements at a bias voltage of 0 V and a frequency of 500 kHz for different oscillator levels.

surements can be found in the Appendix A.2, Figures A.2 to A.5. The systematic errors for this and all following measurements are calculated using data from the official data sheet from Agilent [36]. The statistical error of the capacitance is for all frequencies significantly lower than the systematic uncertainty. This shows that the measurement is very stable and high statistics is not needed for a precise determination of the capacitance. However, it also gives some indication that the statistical spread of the values depends on the frequency and is especially high for very high and low ones, namely 5 MHz and 1 kHz, respectively. The systematic uncertainty also depends on the frequency. For low and high values it is significantly higher than for values between 100 kHz and 1 MHz. Within this range, the measured values for the capacitance are also nearly equal. For very low frequencies the measured capacitance is smaller and for very high ones significantly larger. Thus for all following measurements a frequency of 500 kHz is chosen.
Another variable is the amplitude of the applied oscillating voltage. The result for different levels of the amplitude is given in Table 5.2. The mean values are nearly independent

of the oscillator level, but the spread for individual measurements rises with lower amplitudes. Thus the statistical error for an amplitude of 32 mV is an order of magnitude larger than for 250 mV. An oscillator level of 250 mV is chosen for all following measurements.

### 5.2.2. Voltage sweep

As stated in Chapter 3.4, a change of the capacitance with respect to the applied voltage can yield some information about intrinsic charge carriers in the diamond. For an insulator like unirradiated diamond no free charge carriers and thus no change of capacitance is expected.
For the measurements, the voltage is swept from negative to positive bias voltages and vice versa. As any change of the capacitance with respect to the bias voltage is small, this sweep is repeated several times to reduce the statistical uncertainty. After changing the bias voltage the device waits for 500 ms before measuring the capacitance. The measured values for each voltage step are fitted with a Gaussian distribution to calculate the mean value and its statistical error. As the bias voltage is set to 0 V at the end of each measurement, the B1505A is set to apply the first bias voltage for at least five seconds before starting the next measurement.
Using a non irradiated diamond sample like sample 3, the measurements show the expected behaviour. A voltage sweep from $-500$ V to 500 V is shown in Figure 5.8. The linear fit shows with a slope of $(-2.9 \pm 3.8)$ V/fF that the capacitance of this DUT is stable over the whole voltage range. This means that there are no free charge carriers in the diamond. For the calculation of the mean value, all measured values are histogrammed and fitted with a Gaussian distribution. This yields a capacitance of $(1.3589 \pm 0.0005\ (\text{stat}) \pm 0.0039\ (\text{syst}))$ pF. It is in good agreement with the theoretical value of $(1.3215 \pm 0.0529)$ pF obtained from the physical dimensions of the electrodes and the thickness of the diamond.
For a highly irradiated diamond the assumption of no uncompensated charge carriers in the bulk does not hold true. A characteristic result is given in Figure 5.9. It is clearly visible that the capacitance changes with respect to the bias voltage. Additionally, the measured value for the capacitance depends on the direction of the voltage sweep and shows thus a hysteresis. The change of capacitance is also not monotonously but a bump is visible. The difference between ramping the bias voltage up and down is negligible for values higher than 700 V.
Flipping the diamond, i.e. applying the high voltage on the opposite electrode, shows that the hysteresis of the capacitance is caused by the diamond as other parts of the setup, e.g. the fixture, are not changed. In Figure 5.10 such a measurement is presented. It has

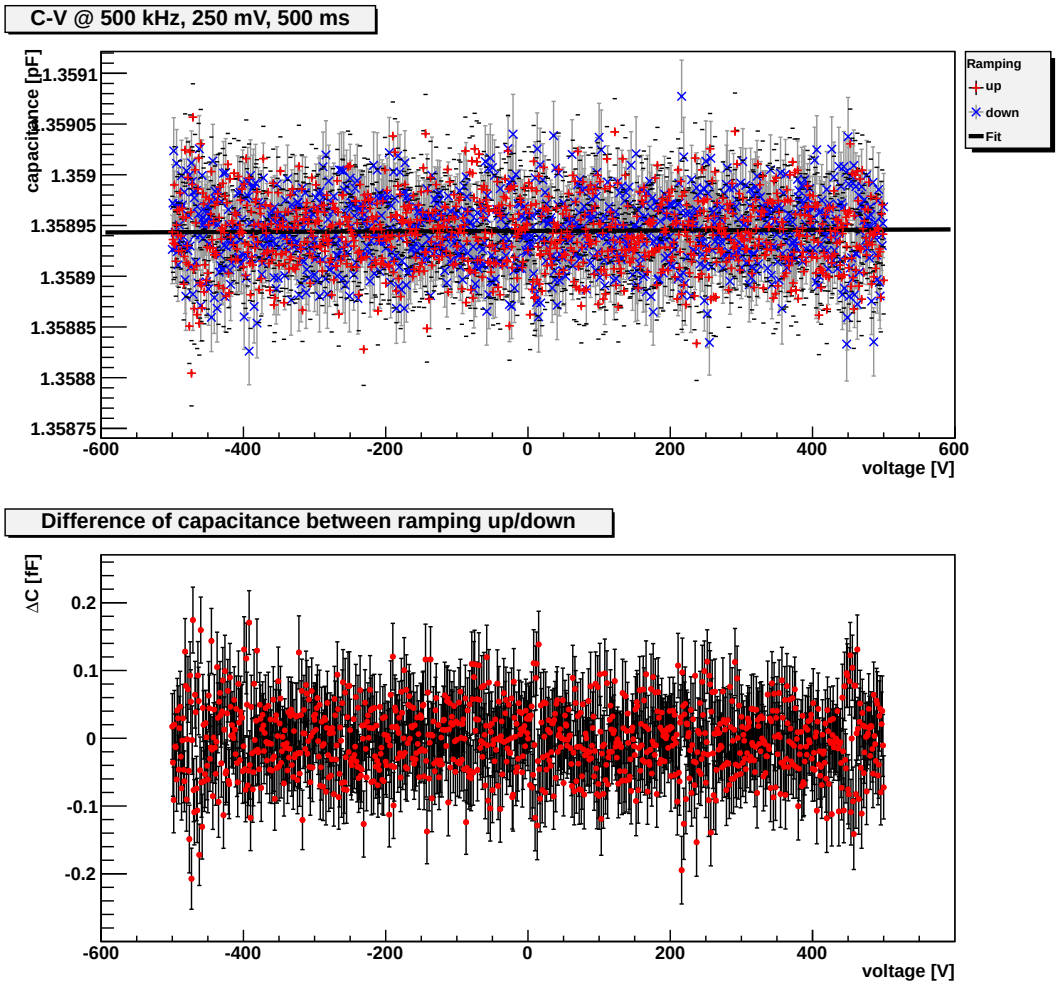


***Figure 5.8.:*** Voltage sweep from −500 V to 500 V for the non irradiated diamond sample 3. The sweep was repeated 235 times. The upper plot shows the measured capacitance for each step with a step size of 1 V. The lower indicates the difference for the values between ramping up and down. Only statistical errors are shown.

the same behaviour of the capacitance with respect to the change of the voltage. The difference of the capacitance compared to the measurement in the original configuration at the same electric field is caused by handling of the diamond and a resulting change of its position inside the fixture rather than by material effects. There is no significant difference for the capacitance between ramping the voltage up and down below a voltage of −700 V. For high positive voltages up to 1500 V the hysteresis is not zero. A slight turn on behaviour is visible for a sweep in positive direction at −1500 V compared to the behaviour of the capacitance at the same field configuration in Figure 5.9. This is due to a polarisation of the diamond. It is lost at the beginning of each sweep due to the inability of the B1505A to hold the bias voltage between two sweeps. In Figure 5.9 this

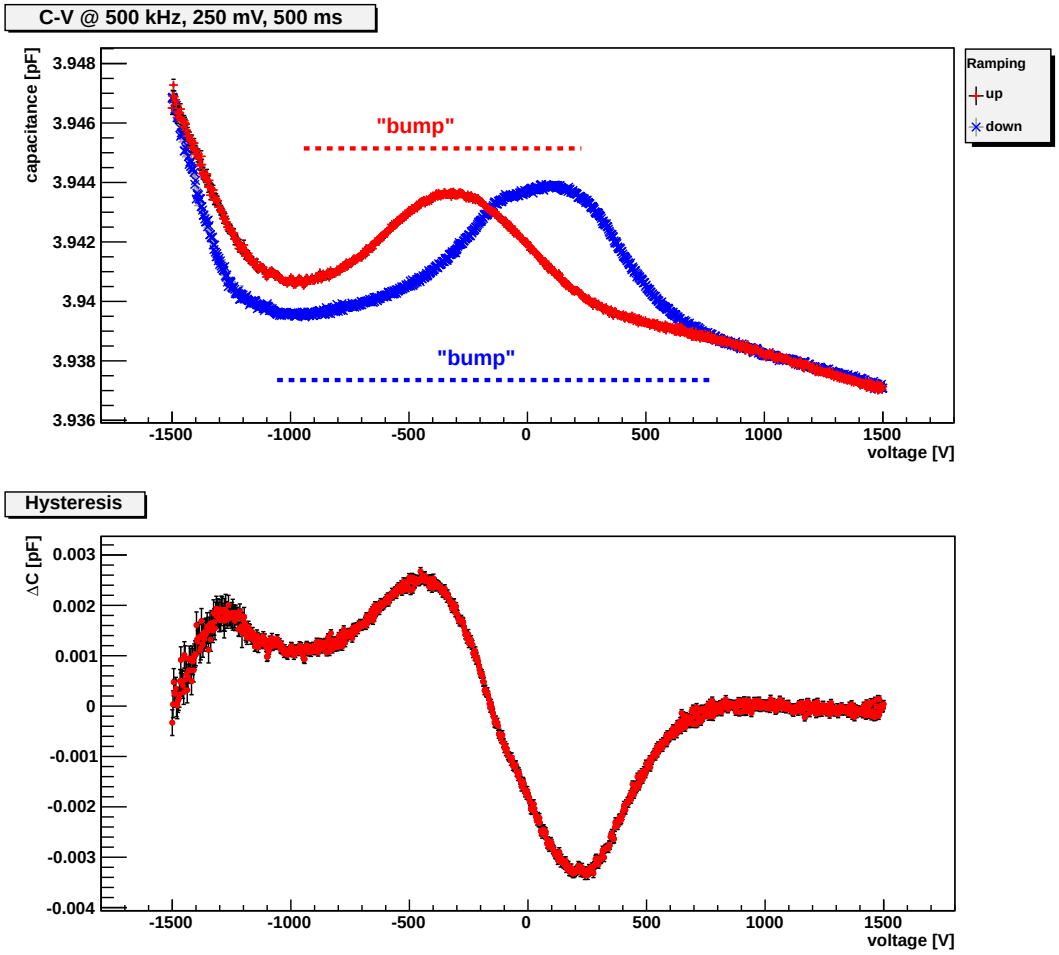


***Figure 5.9.:*** Voltage sweep from −1500 V to 1500 V for the highly irradiated diamond sample 1. The sweep was repeated 122 times. The upper plot shows the measured capacitance for each step with a step size of 3 V. The lower indicates the difference for the values between ramping up and down. Only statistical errors are shown.

could not be seen as it is only a small effect and the capacitance changes more drastically at the begining of the voltage sweep.

According to Equation 3.9 a change of capacitance with respect to the voltage yields information about the number of uncompensated charge carriers in the diamond. This is illustrated in Figure 5.11 for a sweep in positive direction and in negative direction. A combined plot is given in the Appendix in Figure A.6. For this calculation the measurement with the non flipped diamond was used, see Figure 5.9. The derivative of the capacitance with respect to the voltage was calculated using

$$\frac{\mathrm{d}C}{\mathrm{d}V} = \frac{C_{high} - C_{low}}{V_{high} - V_{low}} \,.$$

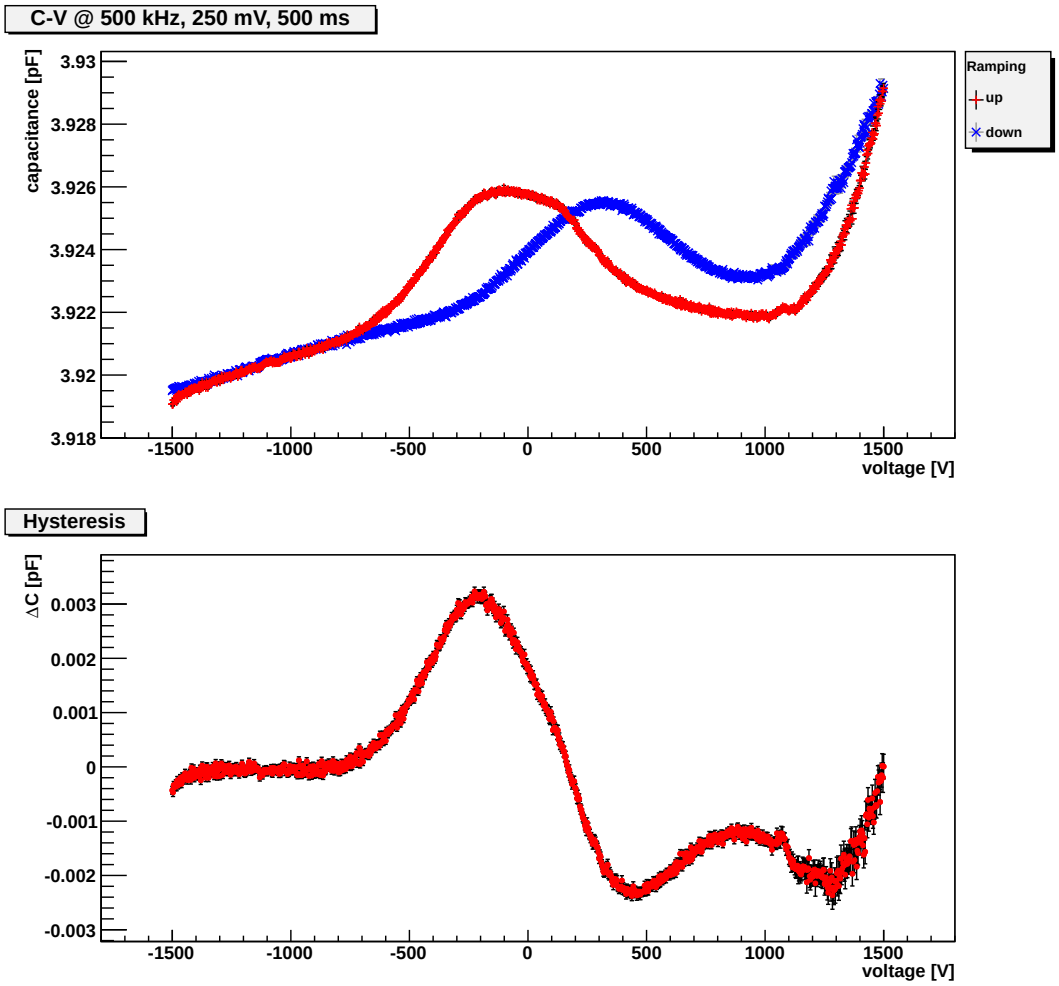


***Figure 5.10.:*** Measurement with the same parameters as in Figure 5.9 but with flipped diamond. This means that the high voltage is applied on the other electrode. The sweep was repeated 139 times. Only statistical errors are shown.

$C_{low}$ is the mean of ten consecutive data points and $C_{high}$ is the mean of the next ten data points. $V_{low}$ and $V_{high}$ are the corresponding mean voltages. The uncertainty on the two mean capacities is quiet high as they cover each a voltage interval of 30 V. Thus, the errors on the uncompensated charges, which are mostly caused by the derivative, are high, too. Also the uncertainty on the size of the electrodes contributes. According to Equation 3.9 the 'bump' results from a sudden change in the sign of the uncompensated charges, which seems unphysical. However, the model was developed for semiconductors with a depleted region so that it does not describe the situation in diamond properly.
The number of uncompensated charges does not vary a lot, especially in the region above 700 V. Here between $2 \cdot 10^{21}$ charges/cm$^3$ and $7 \cdot 10^{21}$ charges/cm$^3$ are measured. This value is quite high considering that diamond should be an insulator and thus have no

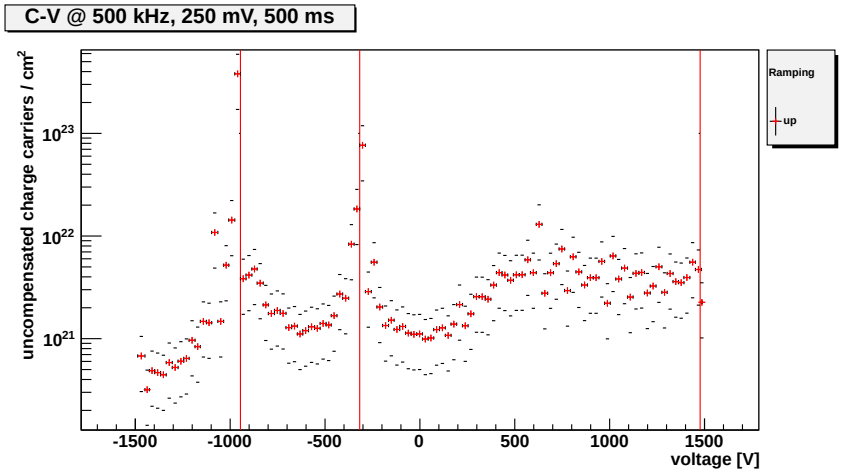


(a) Voltage sweep in positive direction

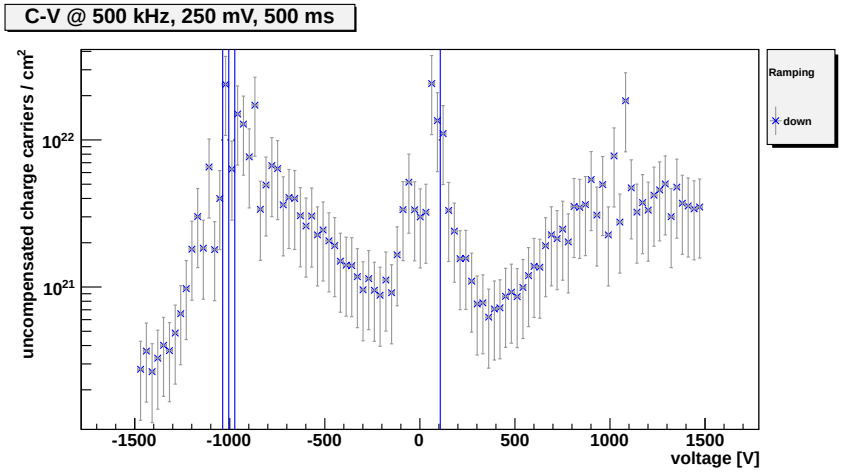


(b) Voltage sweep in negative direction

***Figure 5.11.:*** Uncompensated charges with respect to the bias voltage. A theoretical change of the sign of the uncompensated charge is indicated by vertical lines.

uncompensated charge. It is even orders of magnitude higher than the typical doping concentration in Silicon of $10^{12-16}$ charges/cm$^3$.

Most probably this is caused by the heavy irradiation, which creates vacancies and interstitials which function as charge traps. These defects can contribute as uncompensated charge carriers. The filling and defilling of those traps could explain the overall behaviour of the capacitance with respect to the voltage, especially the hysteresis, if the cross section of the processes changes differently with voltage. However, this does not explain the bump and thus the theoretical change of the sign of uncompensated charge carriers.

A measurement with the diamond being pumped, which is illustrated in Figure 5.12, indicates that the bump may not be caused by the charge traps. In this case the diamond

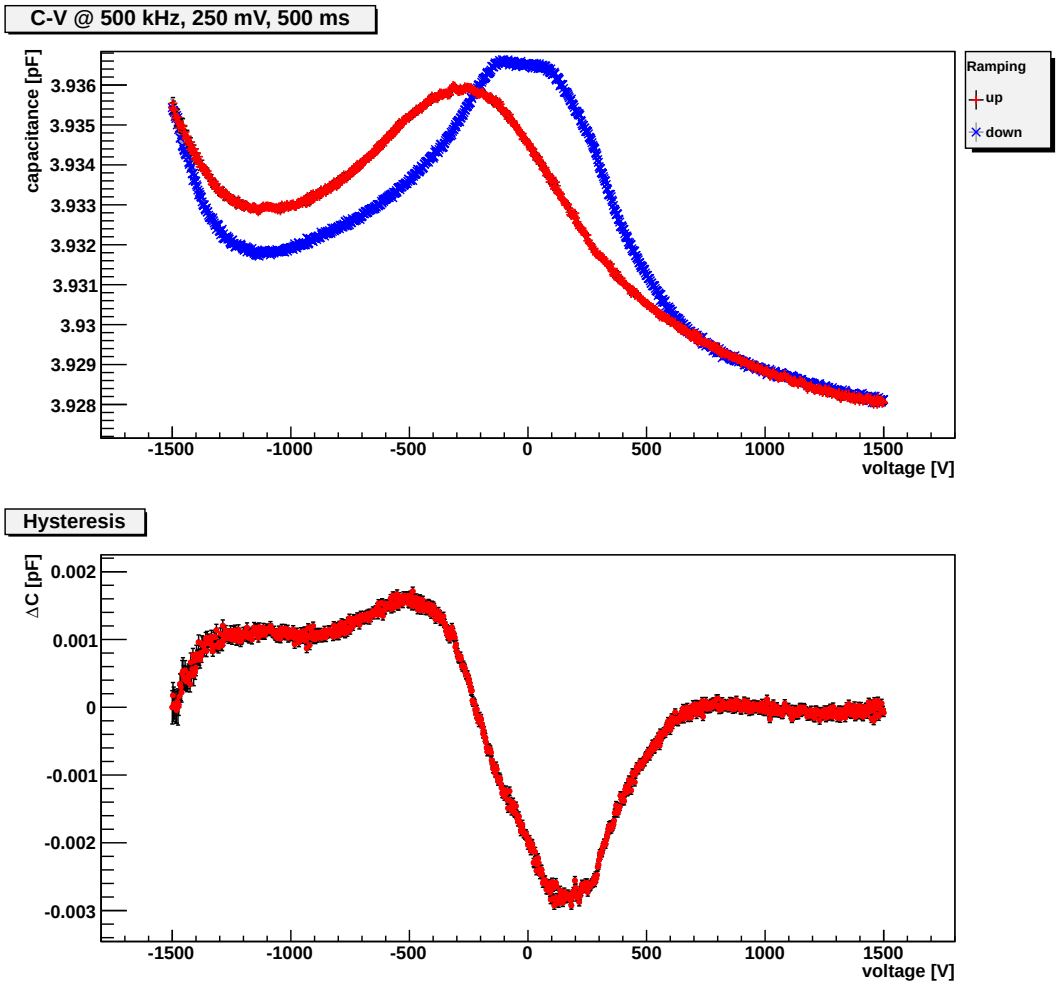


***Figure 5.12.:*** Measurement with the same parameters as in Figure 5.9 but with pumped diamond. The sweep was repeated 185 times. Only statistical errors are shown.

was pumped for six hours with a Sr90 source with an activity of 13.8 MBq to neutralise and thus decrease the number of charge traps. The difference between the measured capacitance at the highest and the lowest voltage of the sweep decreases compared to the unpumped measurement. With a pumped diamond this difference is $(7.54 \pm 0.15)$ fF compared to $(10.26 \pm 0.20)$ fF with an unpumped sample. This indicates that the change of capacitance with respect to the voltage is indeed influenced by the charge traps. Some of them are filled for a pumped sample and thus the number of active charge traps is reduced. The hysteresis itself has a smaller amplitude with 5 fF for the pumped measurement compared to 6 fF for the unpumped sample. This further hints that the hysteresis is caused by the charge traps.

The amplitude of the bump seems not to be influenced by pumping. The difference between the highest capacitance of the bump and the lowest capacitance at negative voltage

is in both cases around 3 fF and 5 fF for a voltage sweep in positive or negative direction, respectively. This bump might be caused by charge traps which have a very short detrapping time or by other effects induced by the high irradiation dose.
Another effect which indicates that the high irradiation dose causes uncompensated charges in the diamond is the capacitance itself. The measured and theoretical values of the unirradiated diamond sample 3 match quiet well as shown before. For the highly irradiated diamond sample 1 the theoretical value is $(3.66 \pm 0.09)$ pF. The larger error on the capacitance of this sample compared to sample 3 is mainly caused by the higher uncertainty on the thickness of the sample. From the measurements an average value of $(3.94 \pm 0.03)$ pF can be obtained. A deviation of these two is noticeable.
This might be caused by using the relative permittivity $\varepsilon_r$ of natural diamond to calculate the theoretical value for this sample. The voltage sweep shows, that this diamond sample has some uncompensated charges. These charges can cause a polarisation and thus increase the value of the relative permittivity. The turn on behaviour at the beginning of the voltage sweep hints at such a polarisation. In contrast, this behaviour is not seen for the unirradiated sample. Thus the irradiation might have changed the relative permittivity of diamond sample 1.

# 6. Measurement of CCD

For the measurement of the CCD a new setup was built. As the deposited charge in diamond is small compared to Silicon, a very low noise level of this setup is required to obtain a signal.

## 6.1. Experimental setup

The setup to measure the CCD of the diamond samples is shown in Figure 6.1(a) and a schematic cut through in Figure 6.2. The samples are put into a fixture inside a metal box. This box works as a Faraday cage to reduce the noise of the setup. The fixture is a Copper clamp which holds the DUT. A photograph of this clamp is given in Figure 6.1(b). During the measurements the box is placed under a plastic tube. This tube holds the radioactive source and a collimator. The tube ensures that the source is in the same position with respect to the DUT. A plastic scintillator is located underneath the box. It is important to reduce the radiation length of this setup to ensure that as many particles as possible traverse the diamond and reach the scintillator. Thus the metal box has two holes above and below the clamp which are covered with thin Aluminium foil. Additionally a hole is drilled through the Copper clamp as the Copper would otherwise shield the diamond from the radiation.
A Sr90 source with an activity of 13.8 MBq is used. The plastic collimator ensures that every particle which hits the scintillator also had to geometrically pass the DUT. It has a thickness of 1 cm and a hole of 1 mm. This reduces the hit rate in the diamond to 3.83 kBq. For a detailed calculation see Appendix A.3.1.
For the read-out of the DUT the clamp is connected with a SHV cable to a charge sensitive preamplifier CSP10 manufactured by Fast ComTec GmbH. The cable has to be as short as possible to reduce the noise pick-up through this connection. To further reduce the noise from the preamplifier its bias voltage is supplied by a low noise power supply. A sketch of the read-out chain is shown in Figure 6.3. The preamplifier has a nominal amplification of 1400 mV per 1 pC.
To reduce the noise a CSA 4 shaper from Fast ComTec GmbH is used. Its available

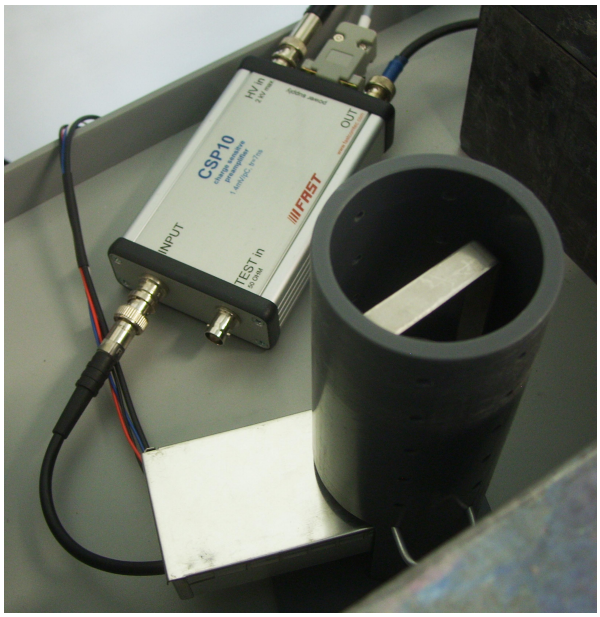


(a) Picture of the plastic tube with source and metal box inserted and the preamplifier. Not visible are the collimator and the scintillator under the box.

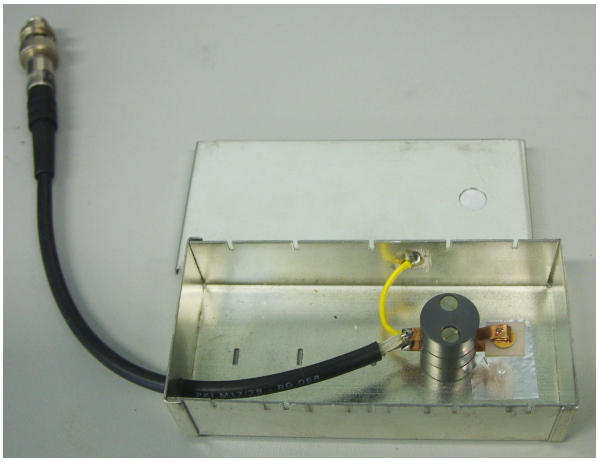

(b) Picture of the fixture for the CCD measurement. The samples are held by a Copper clamp. A hole in the clamp ensures that the material budget of the fixture is as low as possible.

***Figure 6.1.:*** Pictures of the setup.

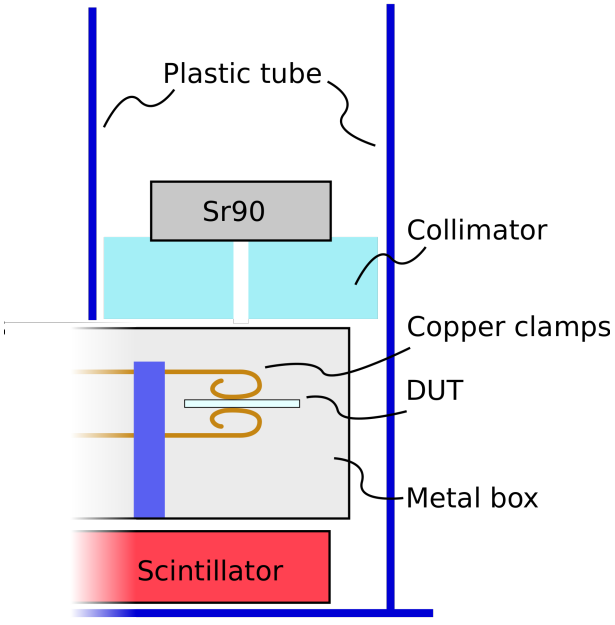


***Figure 6.2.:*** Cut through the setup.

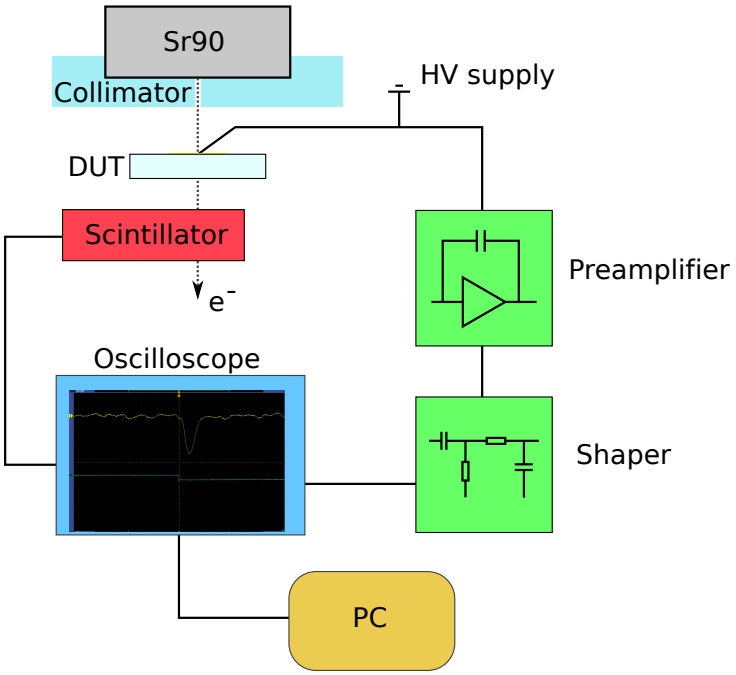


***Figure 6.3.:*** Illustration of the read-out chain. The signal from the diamond is processed in a charge sensitive preamplifier and a shaper. As an external trigger, a scintillator is used. Both signals are recorded by an oscilloscope and transferred to a computer.

shaping times are 100 ns, 500 ns, 2 µs and 8 µs. Additionally, it also amplifies the signal with a nominal gain of 10, 100 or 1000. The preamplifier has a decay time of 140 µs. The signal for each event after the shaper has only a full width at half maximum (FWHM) of 2.4 times the shaping time and thus reduces the likelihood of pile-up effects significantly. The scintillator is used as an external trigger. It has a surface of approximately 1 $cm^2$ and thus covers the whole solid angle seen by the diamond sample. With a thickness of 1 cm it is assumed that it has a detection efficiency of nearly 100% if the rate is not too high for the photomultiplier.

### 6.1.1. Data aquisition & analysis

To read out the signal a Tektronix DSP 4104 oscilloscope is used. It is set to trigger on the signal from the scintillator. The read-out is realised via USB and controlled by a self written LabWindows program. This is either done for each single hit or for the mean value of 128 hits.
For the measurement of the CCD the oscilloscope is set to average over 128 triggered hits. This event is read out and stored with a time stamp. As the averaging is done on the oscilloscope, the information of the single triggered hits is lost. This makes this type of data acquisition vulnerable to inefficiencies of the scintillator. If the scintillator does

not trigger although the diamond sample is hit by a particle, it only reduces the rate but does not influence the measured value. It does influence the measurement, if the diamond sample has no signal from a particle and the scintillator triggers. In this case a pure noise hit is included in the average and thus decreases the mean signal.
To decrease the statistic uncertainty, these events are separated into time intervals. For each of these intervals the mean signal is calculated. Each event has a resolution of 1000 data points which correspond to a time relative to the trigger, i.e. 5 µs before and after the trigger. For every data point, all values from the events within one interval are histogrammed and fitted with a Gaussian distribution. This yields the mean signal from these events and its statistical uncertainty. An example is shown in Figure 6.6.
To calculate the height of this signal, the non-signal region, i.e. between 5 µs and 1 µs before the trigger, is fitted for each interval with a constant to determine the baseline level. As the signal is a negative voltage pulse, this value is subtracted from the lowest measured voltage in the signal region, i.e. between 2 µs and 7 µs after the trigger.
From this voltage the collected charge is calculated. This value is divided by the average number of charges created by a traversing m.i.p. per micrometer, i.e. 36 electrons/µm (see Table 3.1), to obtain the CCD of the sample.
The statistical uncertainty of the CCD is calculated by the uncertainty on the baseline and the uncertainty on the peak value.

## 6.2. Experimental results

### 6.2.1. Calibration

The charge sensitive preamplifier is calibrated by using a test input. A negative voltage pulse is generated by a function generator and applied to the test input of the preamplifier as well as to the oscilloscope. The oscilloscope triggers on this pulse and also records the output of the preamplifier. It automatically computes the mean of the last 512 events. The pulse heights of both pulses are measured using the build-in measurement function of the oscilloscope. The result is presented in Figure 6.4. For a nominal amplification of 1400 mV/pC the test input should be amplified by 6.5 [37]. As the test input is only amplified by $6.304 \pm 0.002$ (see Figure 6.4) this results in a total amplification of $(1358 \pm 1)$ mV/pC. The resulting systematic uncertainty is less than 0.1% and can thus be neglected.
Another systematic uncertainty to consider is the ballistic deficit of the preamplifier. With a saturation velocity for electrons of at least $9.6 \cdot 10^6$ cm/s the charge collection in

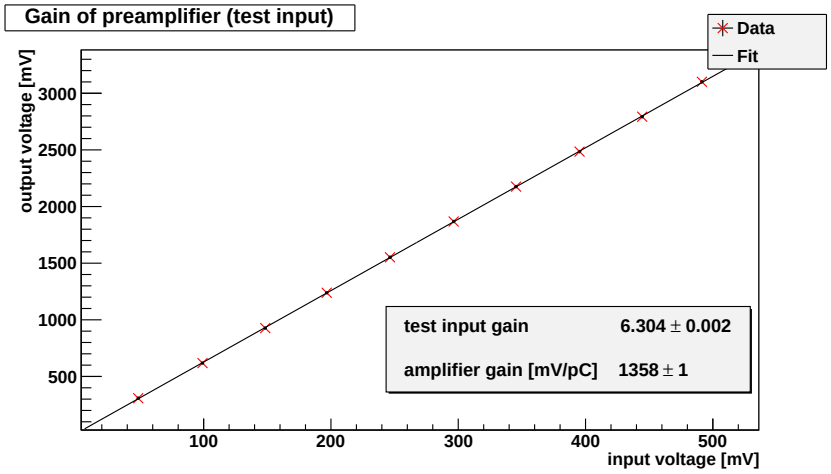


***Figure 6.4.:*** Voltage difference of the output pulse of the preamplifier against input pulse at the test input. Note that the input pulse is negative.

| shaping time [µs] | nominal gain | noise level [mV] |
|---|---|---|
| 0.1 | 100 | 32.0 |
| 0.5 | 100 | 15.6 |
| 2 | 100 | 7.5 |
| 8 | 100 | 11.9 |
| 2 | 10 | 11.7 |
| 2 | 1000 | 7.5 |

***Table 6.1.:*** Noise levels for different settings of the shaper. Note that the levels for a gain 10 and 1000 are normalised to a gain of 100.

a 400 µm thick sample only takes 4.17 ns [5]. Holes are reported to have an even higher saturation velocity. As the feedback capacitor takes 140 µs to discharge, the ballistic deficit can be neglected.

For an effective noise suppression the choice of the shaping time is crucial. To test the noise levels for the different shaping times, diamond sample 1 is put in the fixture and a voltage of 500 V is applied. The scintillator is used as an external trigger. To prevent hits in the DUT the scintillator is not placed far away from the diamond. To trigger it, the source is placed directly above it. The signals from the diamond should now be pure noise and are recorded by the oscilloscope and processed by a PC.

To determine the noise level, the voltage is histogrammed for a period of 10 µs around the trigger, i.e. 1000 data points from each event. At least 500 triggered events are used for the histogramms for each shaping time. These histogramms are fitted with a Gaussian distribution. The results are given in Table 6.1 and the individual plots in Figure A.8 to A.11. For the short shaping times of 0.1 µs and 0.5 µs, the noise level is four and two

times higher than for a shaping time of 2 µs, respectively. At a longer shaping time of 8 µs the noise level increases again. Accordingly for the measurements a shaping time of 2 µs is chosen.
Another parameter of the shaper is the internal gain with nominal settings of 10, 100 and 1000. The noise levels for the different gains are measured with the same method as the noise levels of the shaping time. The results are presented in Table 6.1 and the individual results in Figure A.12 and A.13. For a nominal gain of 10 the noise level is approximately 1.5 times larger than for higher gains. No significant difference in the noise levels for a gain of 100 and 1000 is measured. As for the highest gain the shaper saturates for large pulses, an internal gain of 100 is used for the measurements.
The internal gain can be adjusted via a screw in the shaper and thus this is also calibrated using a function generator. Again the oscilloscope computes the mean of 512 events and the voltage difference. For a nominal gain of 100 an actual gain of $101.6 \pm 2$ is measured. This yields a systematic uncertainty of the shaper of approximately 2%.
The last component to calibrate is the scintillator. The trigger level of the oscilloscope and the supplied voltage of the scintillator are adjusted such that without a source roughly two events per ten seconds are recorded. However, the height of the pulses from the scintillator are altered with time. This is especially drastic in the first 24 hours after changing or turning on the supplied voltage. Accordingly the scintillator is recalibrated after one day and then left unchanged for the measurements. Also removing the metal box and placing it again in the plastic tube without touching or moving the scintillator can in some cases alter its performance. Thus the systematic uncertainty resulting from the scintillator inefficiency is at least on the order of 5 µm CCD due to the averaging on the oscilloscope. It is possible to reduce this uncertainty by using a diamond sample with a high known CCD like e.g. diamond sample 3 and using it as a reference. Unfortunately, the sample was only available for a short time and then the preamplifier broke. Thus, this tuning was not possible.

### 6.2.2. Evolution of CCD with time

While measuring the CCD of a sample the radiation from the source pumps the diamond. Thus an increase of the CCD in time is observed. To ensure that the samples are completely unpumped when starting a measurement they are exposed to a UV-light source for two minutes. The experimental result for diamond sample 2 at a bias voltage of 700 V is given in Figure 6.5.
For analysis the events are split into time intervals of one hour. The CCD is calculated with the method described in Section 6.1.1. An example of the calculated mean signal

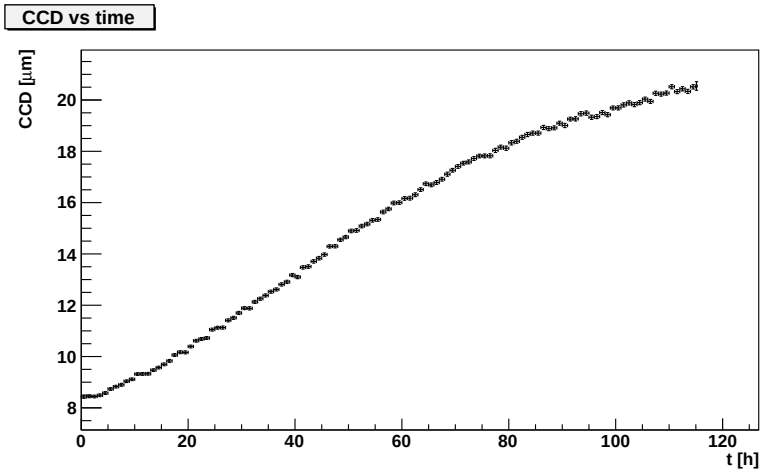


***Figure 6.5.:*** Measurement of CCD of diamond sample 2 over time at a bias voltage of 700 V. Before the measurement the diamond was completely unpumped. An increase of CCD which is interpreted as pumping is visible. Only statistical errors are shown.

for the first hour of the measurement is given in Figure 6.6. The CCD raises in time, at the beginning steeper than after four days.
A similar result is obtained for diamond sample 1. This is shown in Figure 6.7. Even though the increase of CCD with time for this sample is not as steep as for sample 2, it also does not reach saturation after 3 days.
Pumping the DUT during a measurement is very slow as Figure 6.5 shows. Even after five days the CCD does not saturate. Thus to determine the maximum CCD the DUTs are pumped before the measurements by removing the collimator.
A very interesting result is given in Figure 6.8. In this case the diamond sample 2 was held at a bias voltage of 1000 V while being pumped for over 24 hours. Thus it is expected that the DUT is fully pumped and the CCD stable in time. However, in this case the CCD actually decreases in the first few hours. This can be explained by a short detrapping time of certain states at this high voltage, which leads to an overall decrease of filled traps for the reduced particle flow with collimator. This increases the effective number of traps in the diamond and thus decreases the CCD.

### 6.2.3. CCD with respect to the bias voltage

As the velocity of the charge carriers increases with the electric field, a higher field should yield a larger CCD (see Equation 3.1). This increase is not unlimited as the velocity saturates at high fields. This can be seen in Figure 6.9. The values for the CCD are obtained from fully pumped samples.
To measure these values, both samples are set to a bias voltage of 1000 V and pumped

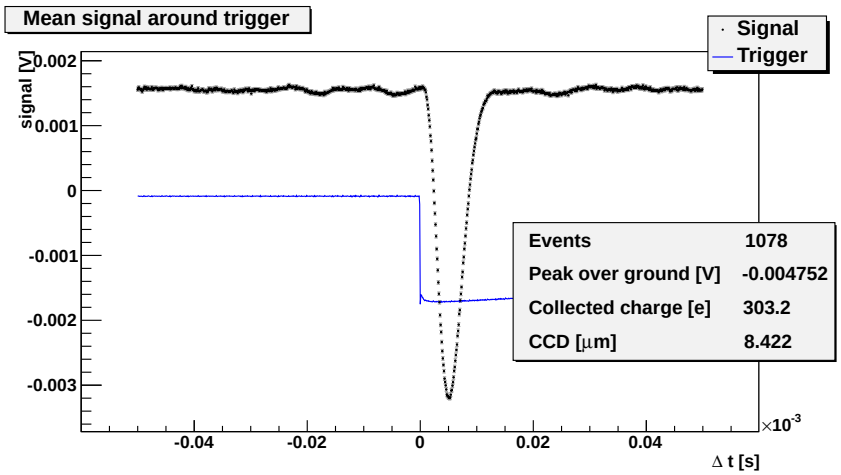


***Figure 6.6.:*** Mean values of all 1078 events from the first hour of the measurement in Figure 6.5. Note that each event already contains the mean values of 128 single events. For each point of the curve, the corresponding data of the 1078 events are histogrammed and fitted with a Gaussian distribution. The mean signal of the trigger is printed in blue.

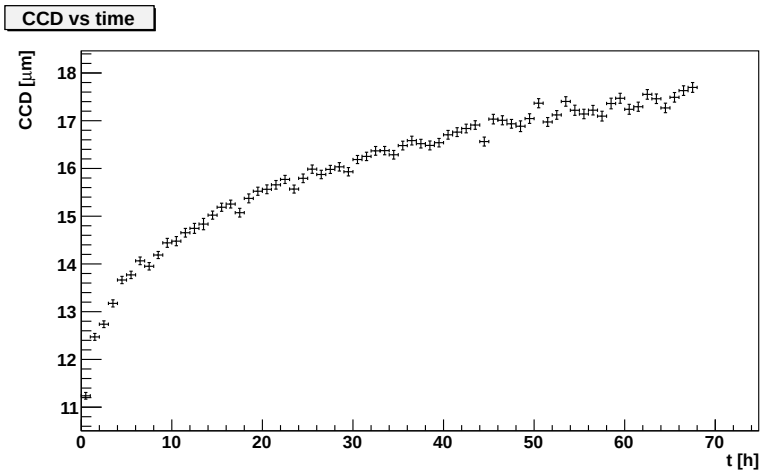


***Figure 6.7.:*** Measurement of CCD of diamond sample 1 over time at a bias voltage of 700 V. Before the measurement the diamond was completely unpumped. An increase of CCD and thus a pumping effect is visible. Only statistical errors are shown.

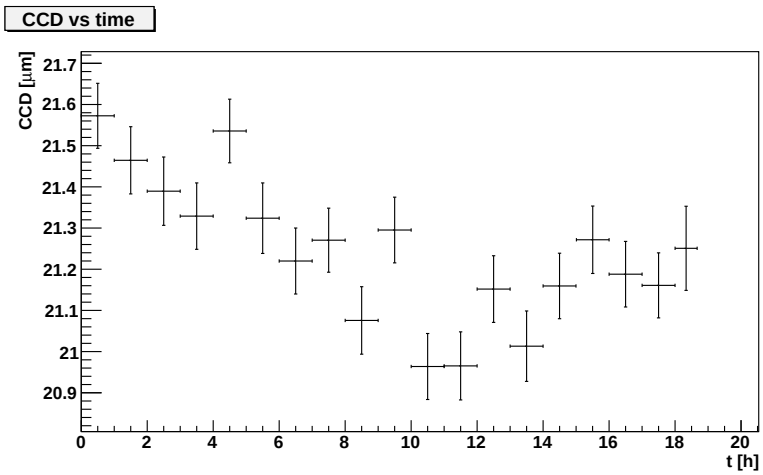


***Figure 6.8.:*** Measurement of CCD of diamond sample 2 over time at a bias voltage of 1000 V. Before the measurement the diamond was pumped for more than 24 hours. A slight decrease of the CCD during the measurement is visible. Only statistical errors are shown.

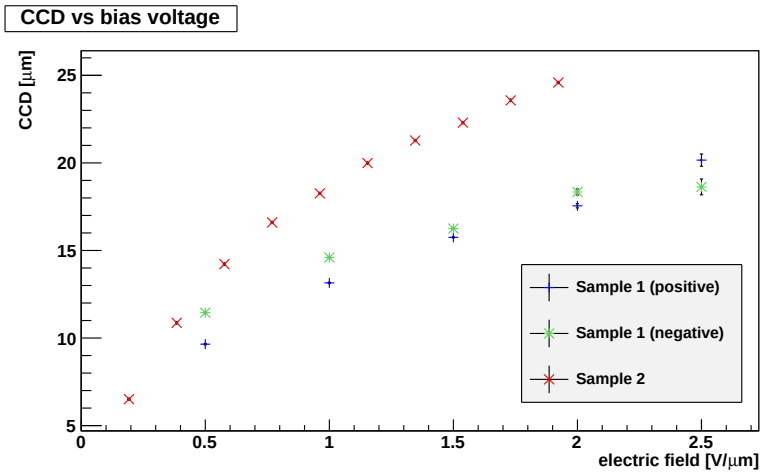


***Figure 6.9.:*** CCD for completely pumped samples with respect to the electric field. For diamond sample 1, a positive and negative bias voltage is applied to collect electrons and holes, respectively. Only statistical errors are shown.

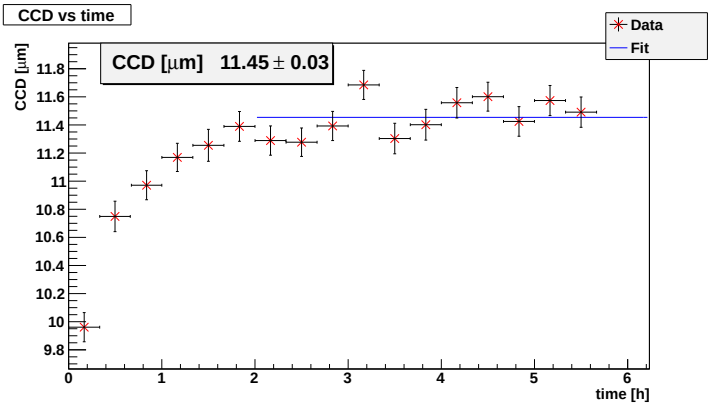


***Figure 6.10.:*** Measurement of CCD of diamond sample 1 over time at a bias voltage of −200 V. Prior to this measurement the diamond was fully pumped at a higher electric field. During the first two hours, an increase of CCD is visible. Only statistical errors are shown.

for at least 24 hours. After the CCD is measured for this voltage for several hours, the voltage is decreased. The removal of the collimator to pump the samples can cause a systematic uncertainty as the metal box and the scintillator might be moved during the removal. Thus the measurements at the lower voltages are done without further pumping. As more charge traps can be filled at a lower electric field, a slight pumping effect for these measurements is observed. An example is given in Figure 6.10. The increase of CCD during the first two hours of the measurement hints that the detrapping time for charge traps might decrease with increasing electric field. For the determination of the saturation CCD the time of pumping is excluded from the linear fit. Plots of the individual measurements with the fit are given in Figure A.14 to A.32.

No clear saturation for the CCD with respect to the voltage is observed up to 1000 V, which corresponds to an electric field of 2.5 V/µm and 1.9 V/µm for diamond sample 1 and 2, respectively. The increase of the CCD is steeper at lower voltages. Even at fairly low voltages and thus small signals, precise values for the CCD are obtained.

For diamond sample 1 both types of charge carriers, electrons and holes, are collected by applying a positive or negative voltage, respectively. In diamond, holes have a higher mobility and thus the CCD is expected to be larger at negative voltages [5]. With exception of the measurement at ±1000 V, this is confirmed by the data.

The larger statistical error at high voltages is caused by the increasing leakage current. Its behaviour for the unpumped diamond sample 1 with respect to the bias voltage is illustrated in Figure 6.11. For this measurement each voltage is applied for ten minutes before measuring the leakage current 300 times. This data is histogrammed and fitted with a Gaussian distribution to obtain the mean value and its statistical error.

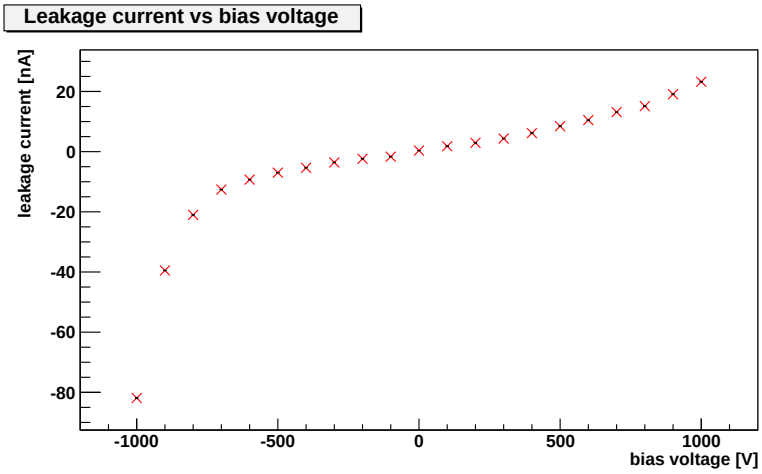


***Figure 6.11.:*** Leakage current as a fuction of the bias voltage for diamond sample 1.

For voltages up to ±500 V, the leakage current increases linearly with the voltage. This is the behaviour of an ohmic resistor. For higher voltages, especially negative, the current rises drastically. As the shot noise is proportional to the square root of the leakage current, measurements of the CCD at high voltages have a higher statistical uncertainty. The values for the CCD have an overall low statistical error of less than 1%. The systematic uncertainty, neglecting the influence of the scintillator, is estimated to be below 2 µm. This uncertainty is due to the handling of the diamond samples and the metal box. As stated above, the uncertainty induced by the scintillator is at least on the order of 5 µm. Furthermore, the values for diamond sample 2 deviate with a factor of 0.5 from values measured at SiLab, University of Bonn [38]. If this is also true for diamond sample 1 cannot be said, as it was not possible to measure any CCD for this sample at SiLab. Thus the setup has to be tuned with another good diamond sample for which the CCD is known for a reference measurement. However, with the current setup it is possible to measure very low values of CCD with a high statistical accuracy.
For diamond samples with a high CCD it is possible to analyse single event data. The data is recorded for each event from the oscilloscope to obtain the full information. For further analysis the local extrema of all events are converted into charges and histogrammed. These local extrema are defined by a minimum voltage difference to the previous one. An example is shown in Figure 6.12. This parameter has to be chosen such that no fluctuations between two points are seen as extrema but the whole noise spectrum is recognized. Thus the value has significant influence on the number of extrema and the charge spectrum. The resulting charge spectrum for a measurement with diamond sample 1 at 700 V is given in Figure 6.13. The Gaussian distribution of the noise is visible. The signal is not separated from the noise.

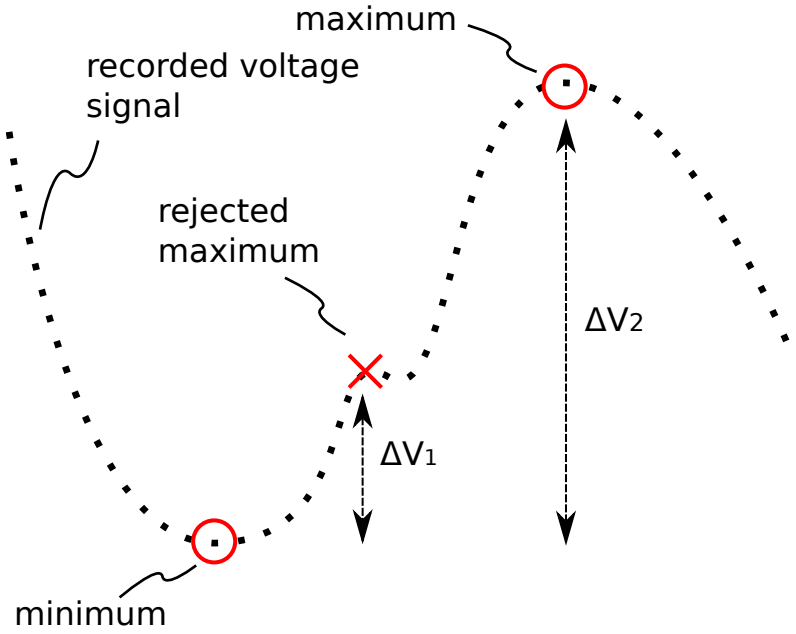


***Figure 6.12.:*** Example of the influence of the minimum voltage difference the local extrema have to have on the recorded charge spectrum. In this example, the threshold is higher than $\Delta V_1$ and lower than $\Delta V_2$. The algorithm searches from left to right. Thus the local maximum with a voltage difference of $\Delta V_1$ is rejected. If the threshold is lower than $\Delta V_1$, the algorithm would record the local maximum and start searching for a minimum. So in this case, the second maximum would not be recorded.

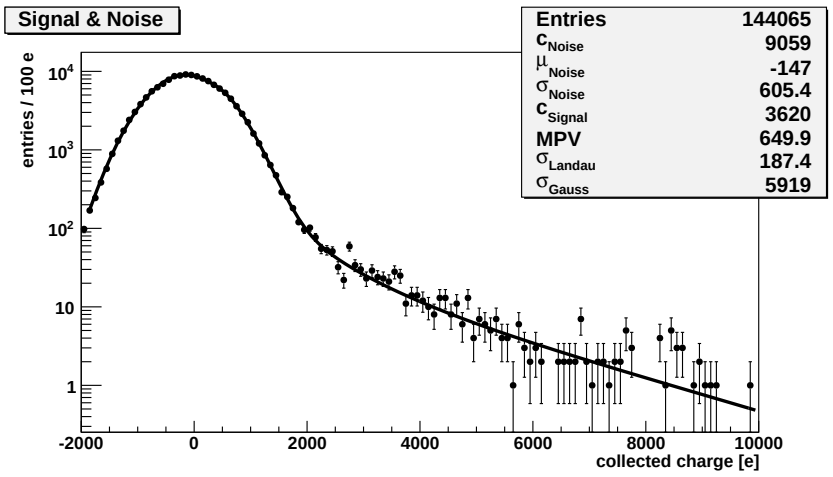


***Figure 6.13.:*** Spectrum of diamond sample 1 at a bias voltage of 700 V. The fit function is given in Equation 6.1.

To analyse this spectrum, in the first step a Gaussian distribution is fitted to the noise spectrum. The fit range is restricted to negative values as this region contains no signal. The whole spectrum is fitted with a convolution of Gaussian and Landau distributions.

$$c_{Noise} \cdot \text{Gauss}\,(\mu_{Noise}, \sigma_{Noise}) + c_{signal} \cdot \text{Landau}\,(\text{MPV}, \sigma_{Landau}) \cdot \text{Gauss}\,(\text{MPV}, \sigma_{Signal}) \quad (6.1)$$

The parameter $\mu_{Noise}$ and $\sigma_{Noise}$ are obtained from the noise fit and are fixed. For the signal, the Landau distribution is convoluted with another Gaussian distribution. This is done as the Landau distribution describes the spectrum only for infinitely thin detectors. The CCD can be calculated via

$$\begin{aligned} \text{CCD} &= \frac{1.22}{36\ \text{e}/\mu\text{m}} \cdot (\text{MPV} - \mu_{Noise}) \\ &= (27.0 \pm 0.8)\ \mu\text{m}\ . \end{aligned}$$

This value is approximately 10 µm larger than the value obtained from the mean values at the same bias voltage.
As the signal is not clearly separated from the noise spectrum, this method has problems with such low CCDs. The fit of the signal is very unstable with small fluctuations of the noise, e.g. varying the threshold for the extrema. Figure 6.13 is one of the few examples where the fit seems reasonable. But for samples with a higher CCD, this method works very well, as only signal events contribute to the signal fit. This eliminates the dependence on the efficiency of the scintillator as its inefficiency only leads to a higher noise peak but does not influence the Landau distribution. Thus, this method can be used as a cross check for the efficiency of the scintillator.

# 7. Graphitisation of diamond using a femtosecond laser

As described in Chapter 4.2, it is possible to induce a phase transformation from diamond to graphite using a femtosecond laser. This method was tested with diamond sample 1. As it is opaque, only graphitisation of the surface is possible. The experimental setup is described in Section 7.1 and the results in Section 7.2.

## 7.1. Experimental setup

A sketch of the experimental setup is shown in Figure 7.1. The laser has a wavelength of 800 fm and is pulsed with a frequency of 1 kHz. Its nominal pulse duration is 30 fs. However, after passing the final lens a pulse duration of 120 ns due to dispersion is expected. The laser has a nominal power of 3 W which results in a power of 25 MW per pulse. It is splitted several times, so that not the full power of the beam is available. To lower the intensity of the beam an attenuator is used, which can be controlled via a PC. To further reduce the intensity the beam passes through a $\lambda/2$-plate and a polariser. These are only used for weakening the beam and not for their primary use. The beam is focused with a lens with a focal length of 5 cm. The diamond can be moved in one

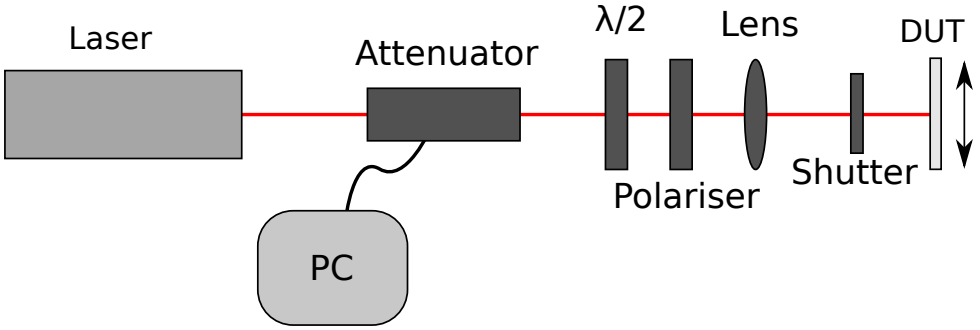


***Figure 7.1.:*** Schematic setup for the graphitisation of diamond. The attenuator is controlled via a PC as well as the horizontal position of the diamond. The focal length of the lens is 5 cm.

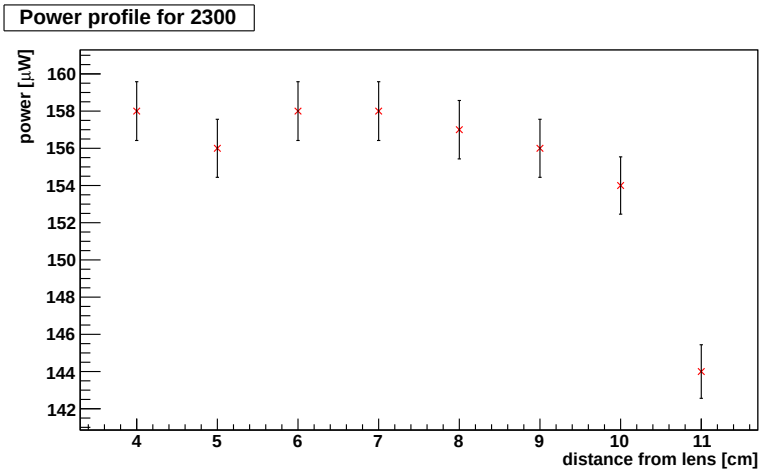


***Figure 7.2.:*** Power profile of the laser beam for an attenuator setting of 2300 au. The power is averaged over one second.

direction perpendicular to the beam with an actuator which is also controlled via a PC. A shutter has to be controlled manually. This makes it impossible to have a shorter duration of exposure of the DUT than 1 s.

## 7.2. Experimental results

### 7.2.1. Calibration

For the graphitisation it is important to know the intensity of the laser beam. As the intensity is controlled by different settings of the attenuator, the power of the laser beam has to be measured for each setting. This is done by putting a power meter into the beam. Due to the pulsing of the laser, the sensor averages the power over one second. The power profile for a certain attenuator setting is illustrated in Figure 7.2. It is stable with distance to the lens up to distances greater than two times the focal length of 5 cm. As the sensor has only a limited active area this may be due to the widening of the beam. Thus, it can be concluded that in the focal region there is no dependence for the power with respect to the distance to the lens.
The power of the laser beam for different settings of the attenuator is shown in Figure 7.3 and summarised in Table 7.1. All measurements were taken in the focal plane. The attenuator shows no linear behaviour.
For calculating the intensity the beam spot size is needed. For an estimation of this, the size of a typical fully graphitised area like in Figure 7.4 is taken. It has a rectangular shape with a short edge of $(23 \pm 2)$ µm and a long edge of $(113 \pm 4)$ µm. This yields a

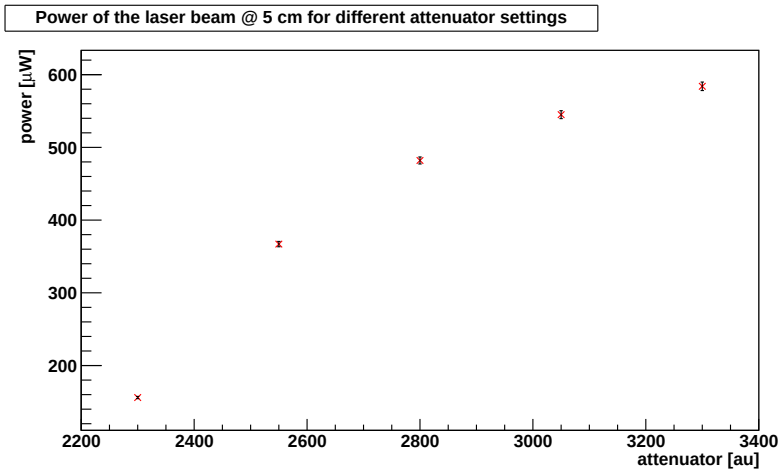


***Figure 7.3.:*** Power of the laser beam for different attenuator settings at the focal point. The power is averaged over one second.

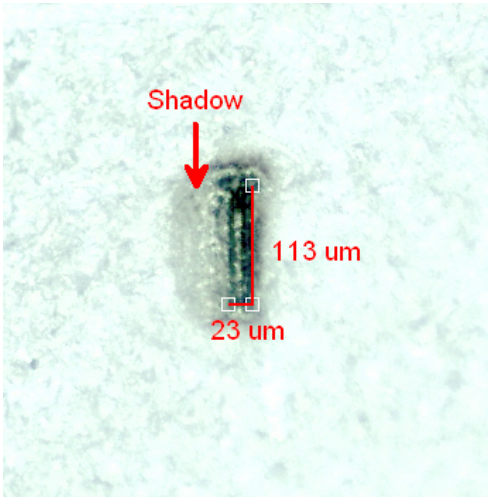


***Figure 7.4.:*** Typical graphite spot after irradiation with the laser beam. The graphitised area has a rectangular shape and a size of $(2.6 \pm 0.2) \cdot 10^{-5}$ cm$^2$. The shadow left of the spot is most probably due to plasma ignited at the diamond surface.

| Attenuator Setting [au] | Power [μW] | Intensity [W/cm$^2$] |
|---|---|---|
| 2300 | $156 \pm 2$ | $6.0 \pm 0.6$ |
| 2550 | $367 \pm 4$ | $14.1 \pm 1.3$ |
| 2800 | $482 \pm 5$ | $18.5 \pm 1.8$ |
| 3050 | $545 \pm 5$ | $21.0 \pm 2.0$ |
| 3300 | $584 \pm 6$ | $22.5 \pm 2.1$ |

***Table 7.1.:*** Power and intensity of the laser beam for different settings of the attenuator. The measurements were taken in the focal plane.

spot size of $(2.6 \pm 0.2) \cdot 10^{-5}$ cm$^2$. The resulting intensity for each attenuator setting is given in Table 7.1.
In Figure 7.4 next to the graphitised area, a slight shadow is visible on the surface of the diamond. This may be caused by a plasma which is ignited when the laser graphitises the diamond on its surface. The graphite absorbs the beam much better than the diamond and is therefore much more heated. This heat might ignite the plasma. Due to a slight tilt of the diamond with respect to the beam direction, the plasma is not uniform around the beam. So the shadow extends more to the left than to the right of the graphite spot.

### 7.2.2. Variable distance to the focal lens

To grow graphite pillars in the diamond, the focal plane needs to be inside the diamond bulk. However, as diamond sample 1 is opaque, the beam is scattered in the diamond. This reduces the intensity of the beam so that the fluence threshold for graphitisation cannot be reached inside the diamond.
Thus for this sample only graphitisation at the surface of the diamond is possible. This also happens only in the focal region as the intensity of the laser beam is otherwise to low.

### 7.2.3. Variable power of the laser beam

To determine the intensity threshold for phase transition on the surface of the diamond, the sample is illuminated at different settings of the attenuator. The result is shown in Figure 7.5. At a power of $(367 \pm 4)$ μW, no transformation is visible. The first visible graphite spot is produced at a power of $(482 \pm 5)$ μW. This corresponds to a power of $(4.0 \pm 0.8)$ kW per pulse. The large error is caused by the uncertainty on the duration of each pulse which is assumed to be at least 20%. Although only very small spots of graphite are visible this is more than twice the power at which graphite pillars can be

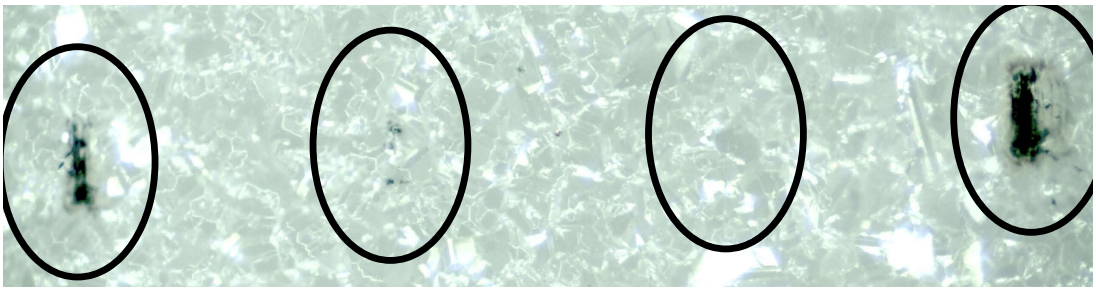

***Figure 7.5.:*** Graphite spots for different powers of the laser beam. From left to right: $(545 \pm 5)$ µW, $(482 \pm 5)$ µW (slightly visible), $(367 \pm 4)$ µW (no transformation visible) and $(584 \pm 6)$ µW. All spots were produced with an exposure time of 10 s, except the last spot which was exposed 20 s to the beam.

grown in monocrystalline diamond, which is 210 µW [33]. The intensity for each pulse - the fluence - at this setting of the attenuator is $(19 \pm 1)$ $\frac{\mathrm{J}}{\mathrm{cm}^2}$. This value is more than an order of magnitude higher than the upper threshold for continuous growth of graphite, which is $(1.2 \pm 0.2)$ $\frac{\mathrm{J}}{\mathrm{cm}^2}$ [32]. Thus, phase transition from diamond to graphite is expected at much lower power.

There are several explanations for the observed higher threshold. On the one hand, all results from publications were produced using monocrystalline and not polycristalline diamond like sample 1. However, due to grain boundaries in polycrystalline diamond, the threshold for graphitisation is expected to be lower. On the other hand, the monocrystalline diamonds were of optical quality which may support graphitisation at lower powers. The measured power threshold does not differ that much from the expectation compared to the measured fluence. This may indicate that the focused beam might be wider than the graphite spots indicate.

However, the power threshold for graphitisation in the bulk of this sample can even be a little higher for two reasons. Single hot, i.e. high energetic, electrons are needed as a seed for the avalanche ionisation causing the phase transition. Due to the incomplete crystal lattice at the surface and at grain boundaries it might need less energy to create these seed electrons. Additionally, all these spots were produced on the growth side of the diamond, which is not even. This can be seen e.g. in Figure A.1. The rough surface might cause some reflections and thus increase the fluence locally. This increased local fluence can create small nano sized graphite grains at grain boundaries. At these graphite spots it takes much less energy to create a seed electron as graphite has no band gap. Thus, once a nano sized graphite grain is created it grows with each shot even at energies below the nominal threshold.

For a power setting of $(545 \pm 5)$ µW, nearly complete graphitisation of the spot size at

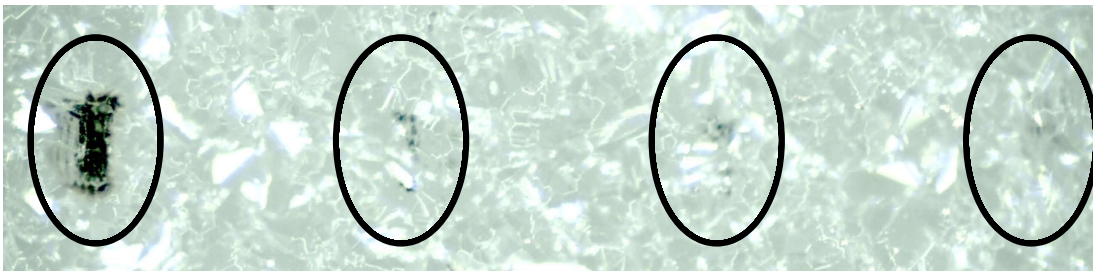

***Figure 7.6.:*** Graphite spots for different times of exposure to the laser beam. From left to right: $(584 \pm 6)$ µW for 3 s, $(482 \pm 5)$ µW for 60 s, 40 s and 20 s (no transformation visible).

the surface is observed. For the graphite spot produced with a power of $(584 \pm 6)$ µW, an even larger fraction of the surface is graphitised. In this case, the shadow caused by the plasma is visible again.

### 7.2.4. Variable duration of exposure

The initial formation of graphite depends entirely on the fluence of each single shot. As the transformation happens on the timescale of one shot, it is not possible for effects from consecutive shots to pile up. The number of shots and thus the duration of exposure to the beam can only control the size of the graphitised volume.
This dependence is illustrated in Figure 7.6. It is clearly visible that with increasing duration of exposure of the diamond, the graphite spots grow larger at a power of $(482 \pm 5)$ µW. While after 20 s no graphite can be spotted, the graphite grains grow larger for 40 s and 60 s. This slow growth indicates that at this power level the threshold for phase transition at the surface is barely reached. Furthermore, this measurement hints that the threshold might even be a little higher. As explained above, due to reflections a higher local fluence can create nano sized graphite spots at grain boundaries. The spot with 20 s of exposure is located on a relative big diamond grain, such that no nano sized graphite spot was created. This would explain, why in this case no graphite is visible, but in Figure 7.5 for 10 s some graphite is produced.
As expected for lower laser power, no phase transition even after an exposure time of more than 2 min is observed. Going to higher powers significantly speeds up the formation of graphite. In Figure 7.7, different durations of exposure for a power of $(584 \pm 6)$ µW are shown. No significant difference is visible between these spots. It can be concluded that at this power level the full graphitisation of the focal area takes less than a second.

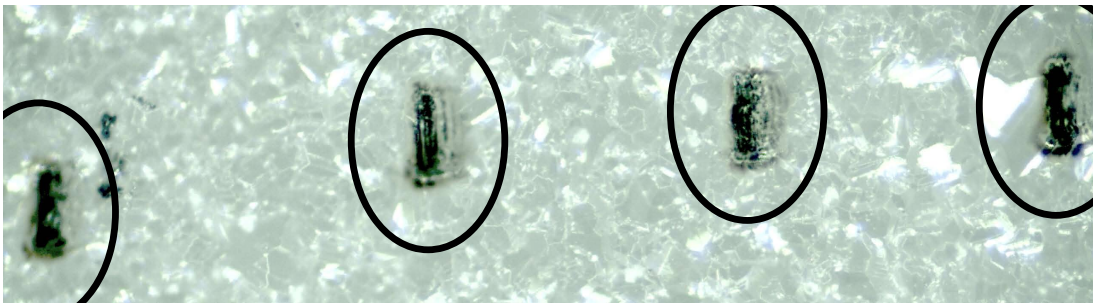

***Figure 7.7.:*** Graphite spots for different times of exposure to the laser beam. From left to right: $(584 \pm 6)$ µW for 10 s, 1 s, 2 s and 5 s.

### 7.2.5. Depth of graphite spots

For three dimensional electrodes the graphite has to be produced within the diamond bulk. So an interesting question is how deep the graphite grows even when the focus is on the surface of the diamond sample. To investigate this, the laser is focused at the edge of the test sample. The resulting graphite spots on the surface at a power of $(584 \pm 6)$ µW are shown in Figure 7.8 (a). As only a part of the laser spot is on the diamond when looking from the side, the depth of the graphite spot can be measured. This is illustrated in Figure 7.8 (b). The graphite is nearly exclusively produced on the surface. Its depth is below the resolution of the microscope.
This result is expected as the diamond is optically dense at the wavelength of the laser and thus even if the focus is inside the diamond bulk, graphitisation can only happen on the surface. Additionally, once graphite is produced on the surface it absorbs the laser further reducing the intensity in the diamond bulk.

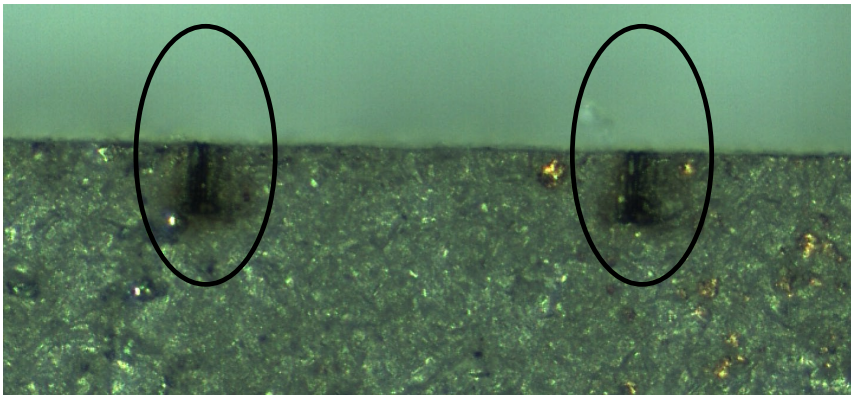

(a) Look on the surface ot the substrate side.

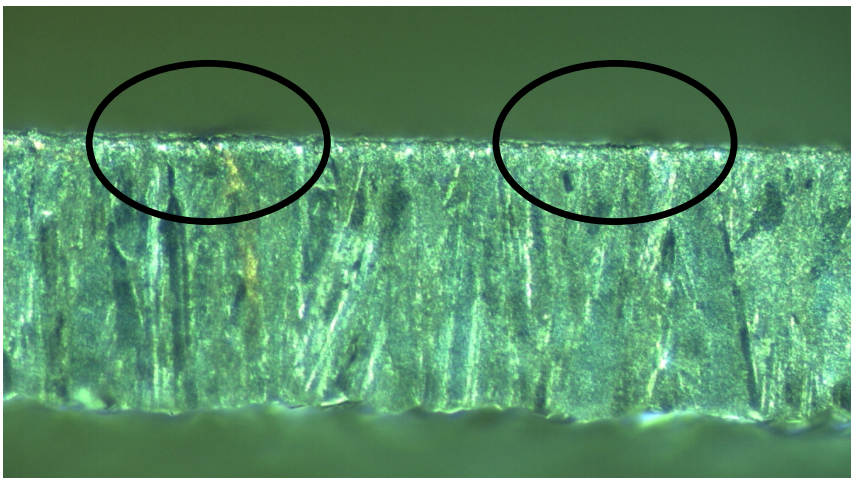

(b) Picture of the two spots from the side. The substrate side is on the top and the growth side at the bottom.

***Figure 7.8.:*** Two graphite spots produced with a power of $(584 \pm 6)$ µW at the edge of the diamond sample. The phase transformation is only induced at the surface and not in the bulk of the diamond.

# 8. Conclusion & Outlook

The results presented in this thesis show that diamond can be used as a sensor material even after high radiation doses.
The measurements of the capacitance with respect to the bias voltage show, that for highly irradiated diamonds the capacitance shows hysteresis effects. This is caused by the charge traps which are a result of the irradiation. Thus the CV measurement can be used to determine the quality of irradiated diamond samples.
The CCD measurements show, that samples with very low CCD at low voltages can be measured with a high statistical accuracy. Even from samples which cannot be measured with other setups, a CCD can be extracted. The setup was designed to have a very low noise level as the voltage signal in diamond is very small. The only remaining problem is the trigger efficiency of the scintillator because it has direct influence on the measured value of the CCD. As it was not possible to tune the whole setup with a diamond sample with a high known CCD, the systematic uncertainty is still quiet high.
The influence of pumping was observed in both measurements. As the pumping fills the charge traps, the hysteresis of the capacitance with respect to the bias voltage decreases and the CCD increases. An indication that a high particle flux is needed to fully pump a highly irradiated sample was found. The shortest detrapping time in this measurement was on the order of hours.
The graphitisation process of diamond using a femtosecond laser for three dimensional sensors was tested successfully. As an opaque diamond sample was used, only graphitisation on the surface was observed. The threshold of surface graphitisation for this sample was determined to be at least $(482 \pm 5)$ µW.
For graphitisation inside the diamond bulk a sample of optical quality is needed as well as a mechanism to move the sample in all three dimensions. Also a shutter to control the duration of exposure has to be installed.

# A. Appendix

## A.1. Pictures of the diamond

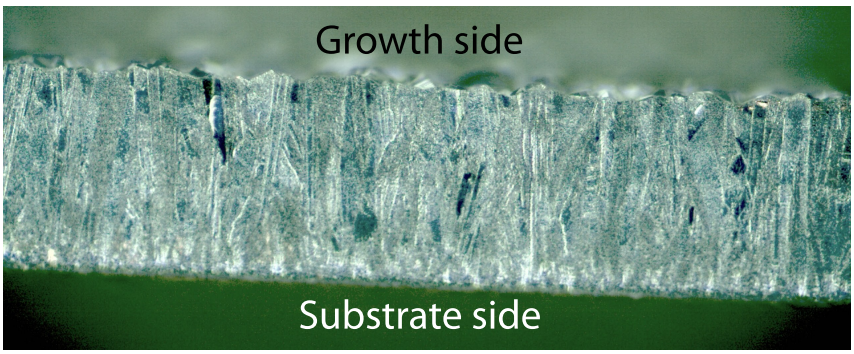


***Figure A.1.:*** Picture of one edge of diamond sample 1 (see Section 5.1.3). The growth side (top) is clearly rougher than the substrate side (bottom).

## A.2. C-V measurement

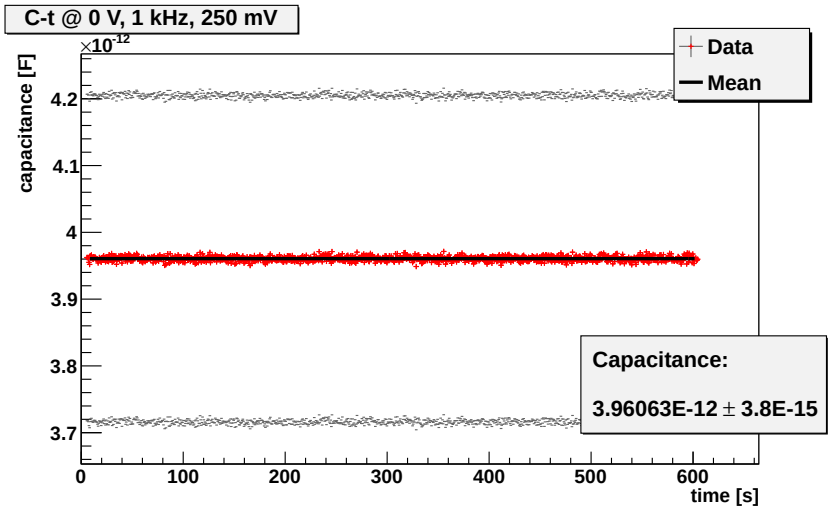


***Figure A.2.:*** Measurement of capacitance at a constant bias voltage of 0 V and a frequency of 1 kHz. The error for each data point indicates the systematic uncertainty. The error on the capacitance is the statistical error.

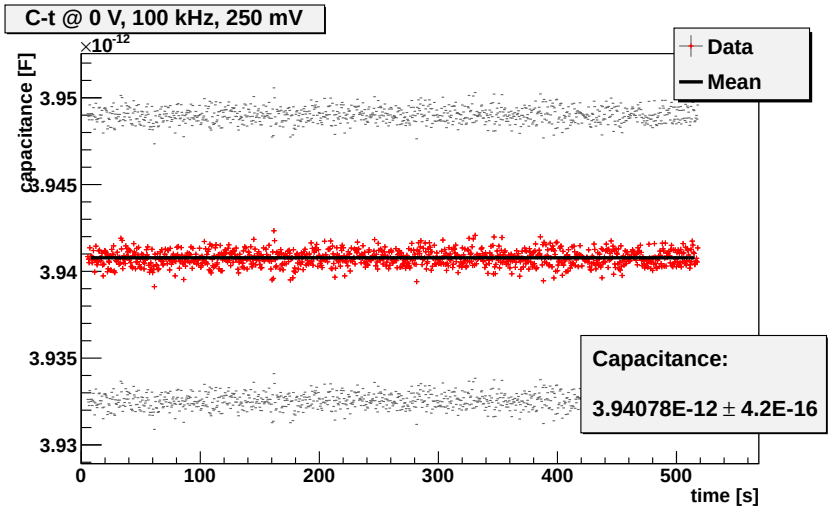


***Figure A.3.:*** Measurement of capacitance at a constant bias voltage of 0 V and a frequency of 100 kHz. The error for each data point indicates the systematic uncertainty. The error on the capacitance is the statistical error.

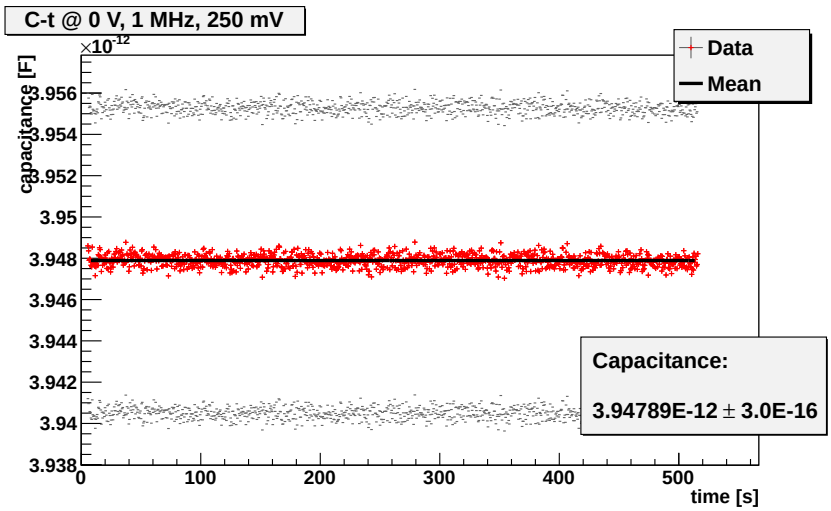


***Figure A.4.:*** Measurement of capacitance at a constant bias voltage of 0 V and a frequency of 1 MHz. The error for each data point indicates the systematic uncertainty. The error on the capacitance is the statistical error.

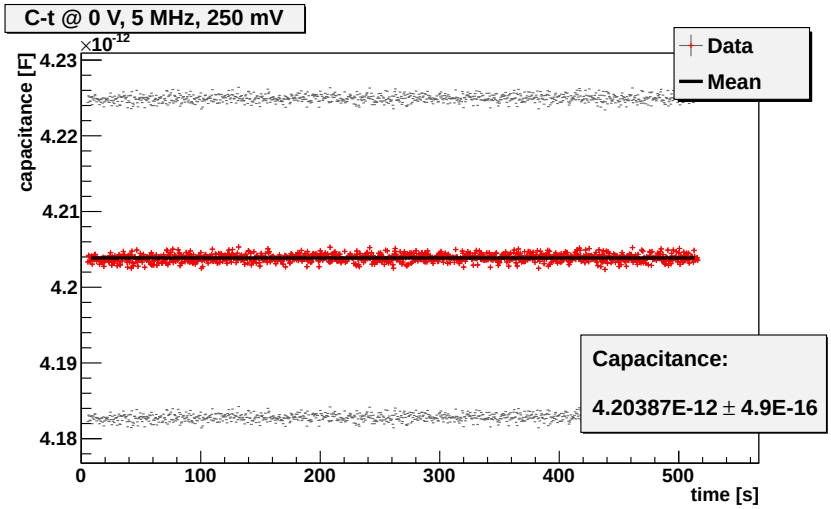


***Figure A.5.:*** Measurement of capacitance at a constant bias voltage of 0 V and a frequency of 5 MHz. The error for each data point indicates the systematic uncertainty. The error on the capacitance is the statistical error.

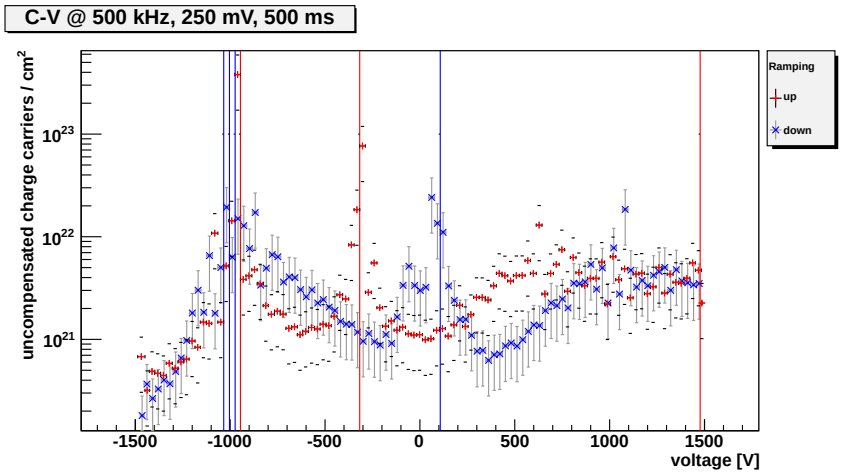


***Figure A.6.:*** Uncompensated charges as a function of the bias voltage. A change of the sign of the uncompensated charge according to the theoretical model is indicated by vertical lines in the colour of the direction of the voltage sweep.

# A.3. CCD measurement

## A.3.1. Calculation of activity after collimator

To be able to calculate the efficiency of the DUT it is important to know the particle flux after the collimator. The nominal activity of the source of $A_{nom} = 13.8$ MBq is emited from a small grain of Strontium. The task is to calculate the fraction of particles which pass the collimator. For the calculation it is assumed that the source is point like. A sketch of the source and the collimator is given in Figure A.7. The grain does not directly face the collimator but is located in a recess at a distance of $a = 5$ mm from it. The collimator itself has a thickness of $D = 10$ mm and the circular hole a diameter of $d = 1$ mm. Thus the angle $\alpha$ can be calculated via

$$\alpha = 2 \arctan \frac{d/2}{D + a} \ .$$

To determine the ratio of particles which are emitted within the opening angle of $\alpha$ with respect to the full solid angle of $4\pi$ the surface of the spherical cap $A_{sur}$ has to be known. It can be calculated via [39]

$$A_{sur} = 2\pi r^2 \left(1 - \cos \frac{\alpha}{2}\right) \ .$$

$r$ is the radius of the sphere. With the surface of the spherical cap, its solid angle $\Omega$ is determined by

$$\Omega = \frac{A_{sur}}{r^2} \ .$$

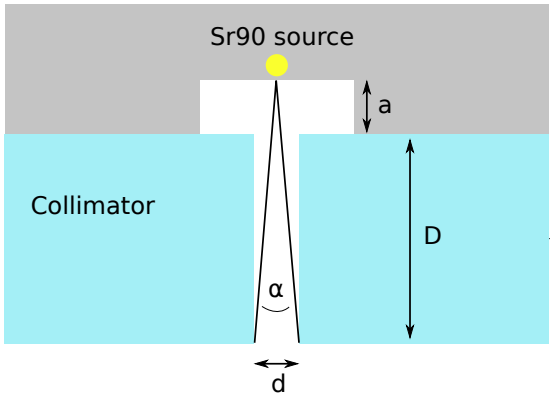


***Figure A.7.:*** Sketch of the source facing the collimator. The opening angle is indicated with $\alpha$.

Thus the effective activity $A_{eff}$ after the collimator is

$$\begin{aligned} A_{eff} &= \frac{A_{nom}}{2}\left(1-\cos\left(\arctan\frac{d/2}{D+a}\right)\right) \\ &= 3.83\ \text{kBq}\ . \end{aligned}$$

## A.3.2. Shaper calibration

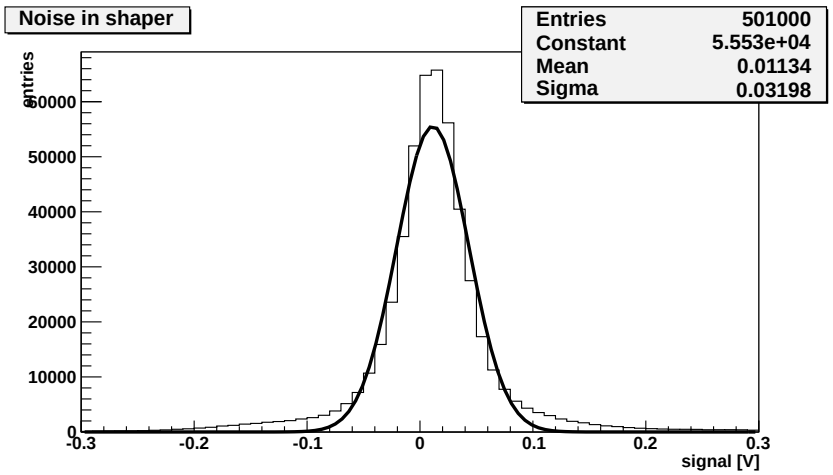


***Figure A.8.:*** Noise after the shaper with diamond sample 1 connected and a bias voltage of 500 V. The shaper was set to a shaping time of 0.1 µs and a nominal gain of 100. In this case two different sources of noise are visible. The dominating source has a much lower noise level than the suppressed source.

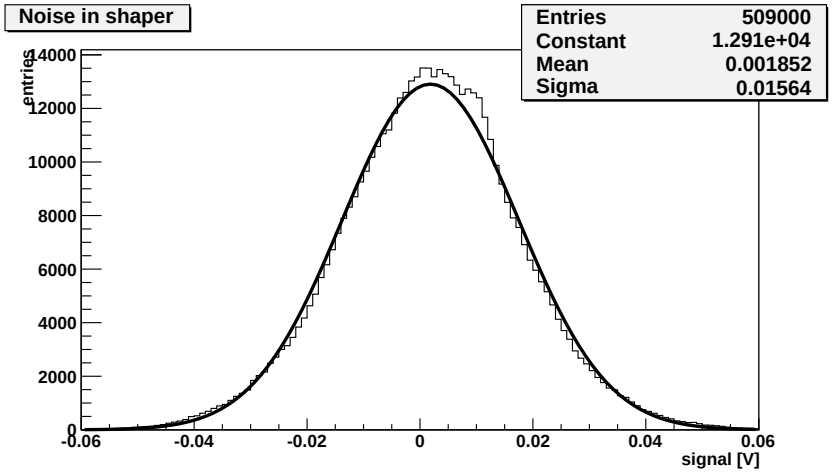


***Figure A.9.:*** Noise after the shaper with diamond sample 1 connected and a bias voltage of 500 V. The shaper was set to a shaping time of 0.5 µs and a nominal gain of 100.

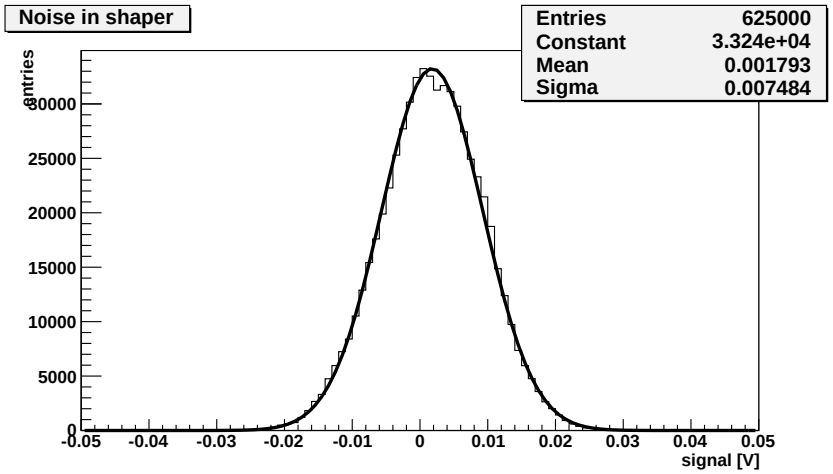


***Figure A.10.:*** Noise after the shaper with diamond sample 1 connected and a bias voltage of 500 V. The shaper was set to a shaping time of 2 µs and a nominal gain of 100.

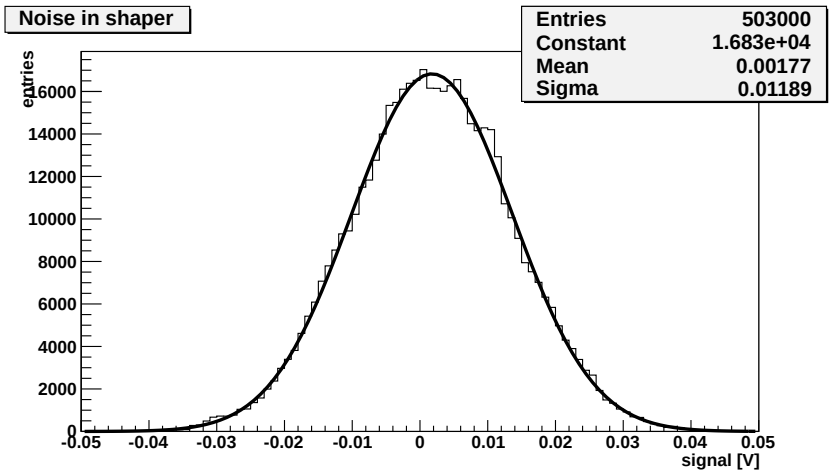


***Figure A.11.:*** Noise after the shaper with diamond sample 1 connected and a bias voltage of 500 V. The shaper was set to a shaping time of 8 µs and a nominal gain of 100.

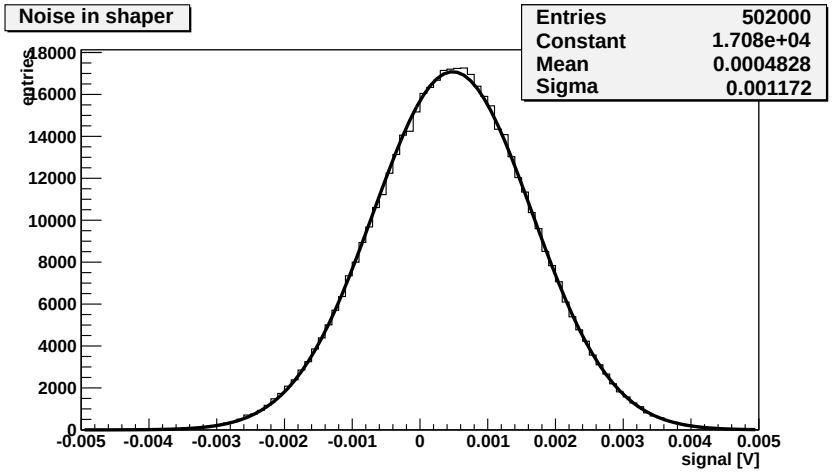


***Figure A.12.:*** Noise after the shaper with diamond sample 1 connected and a bias voltage of 500 V. The shaper was set to a shaping time of 2 µs and a nominal gain of 10.

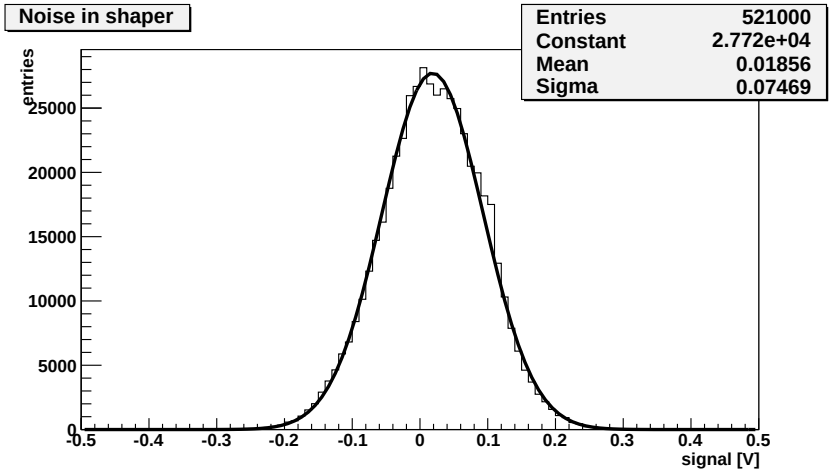


***Figure A.13.:*** Noise after the shaper with diamond sample 1 connected and a bias voltage of 500 V. The shaper was set to a shaping time of 2 µs and a nominal gain of 1000.

### A.3.3. CCD with respect to the bias voltage

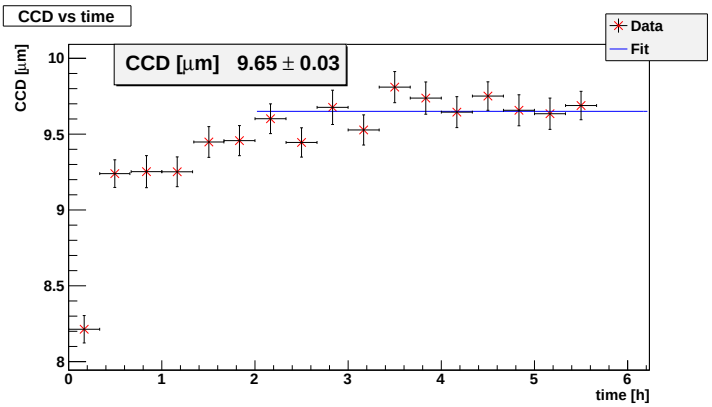


***Figure A.14.:*** Measurement of CCD of diamond sample 1 over time at a bias voltage of 200 V. Only statistical errors are shown.

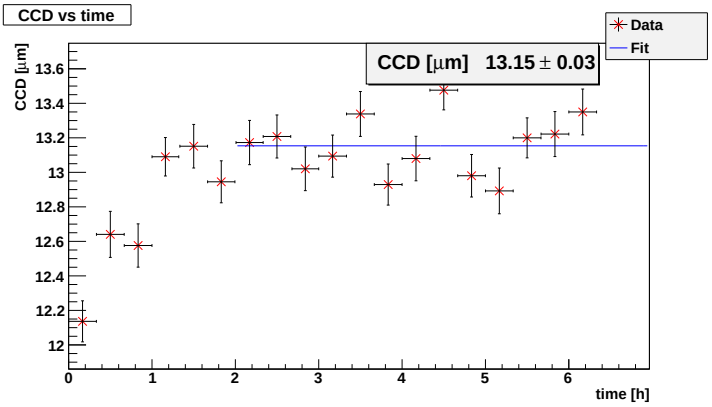


***Figure A.15.:*** Measurement of CCD of diamond sample 1 over time at a bias voltage of 400 V. Only statistical errors are shown.

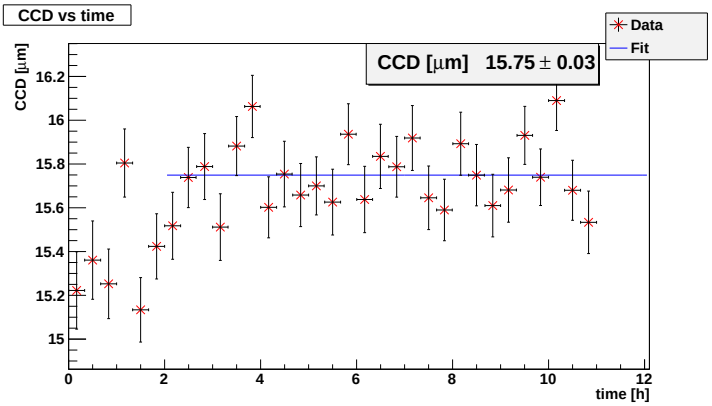


***Figure A.16.:*** Measurement of CCD of diamond sample 1 over time at a bias voltage of 600 V. Only statistical errors are shown.

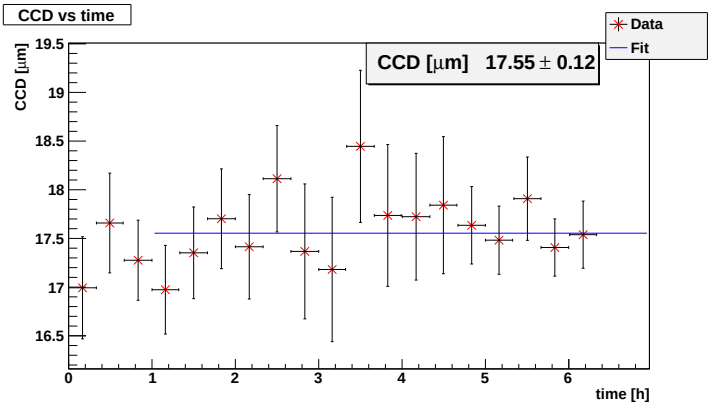


***Figure A.17.:*** Measurement of CCD of diamond sample 1 over time at a bias voltage of 800 V. Only statistical errors are shown.

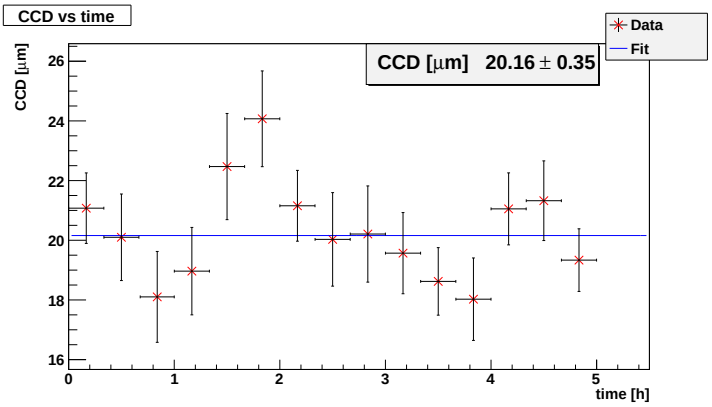


***Figure A.18.:*** Measurement of CCD of diamond sample 1 over time at a bias voltage of 1000 V. Only statistical errors are shown.

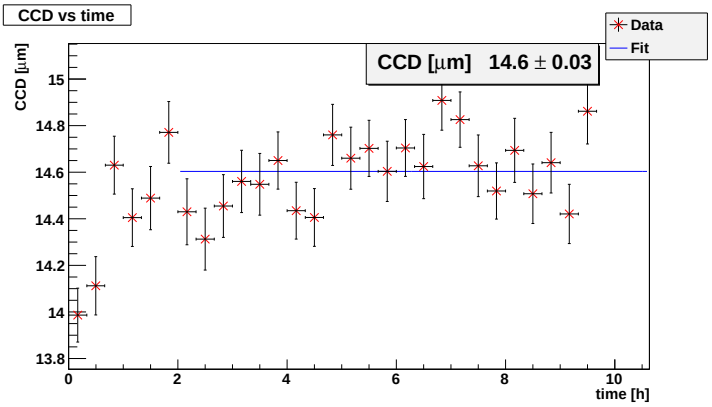


***Figure A.19.:*** Measurement of CCD of diamond sample 1 over time at a bias voltage of −400 V. Only statistical errors are shown.

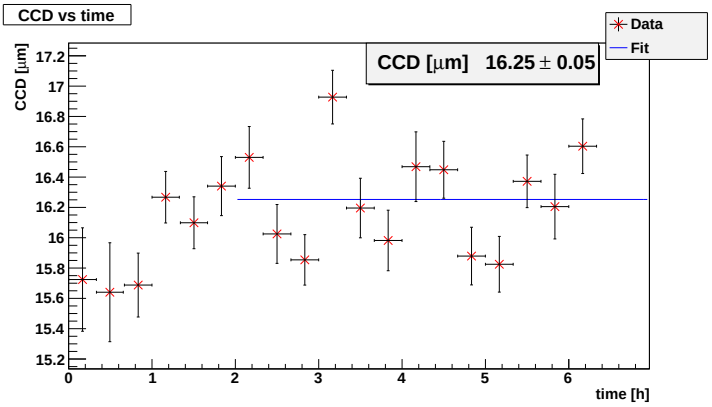


***Figure A.20.:*** Measurement of CCD of diamond sample 1 over time at a bias voltage of −600 V. Only statistical errors are shown.

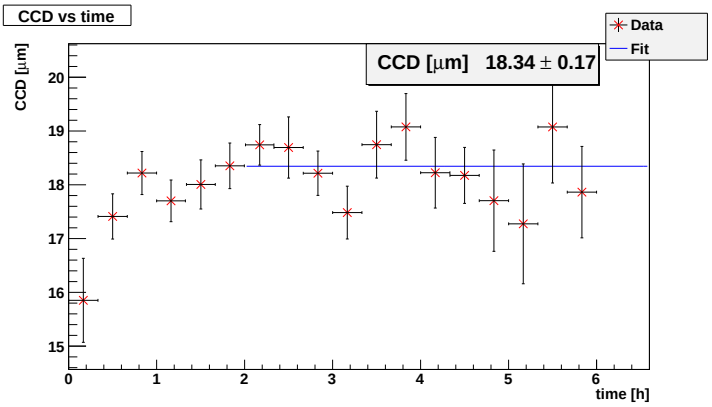


***Figure A.21.:*** Measurement of CCD of diamond sample 1 over time at a bias voltage of −800 V. Only statistical errors are shown.

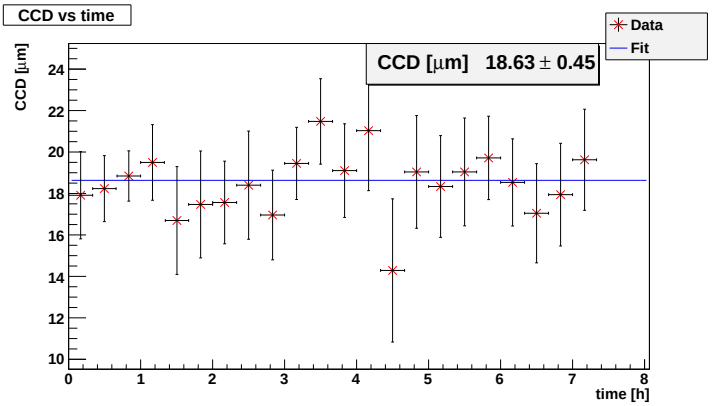


***Figure A.22.:*** Measurement of CCD of diamond sample 1 over time at a bias voltage of −1000 V. Only statistical errors are shown.

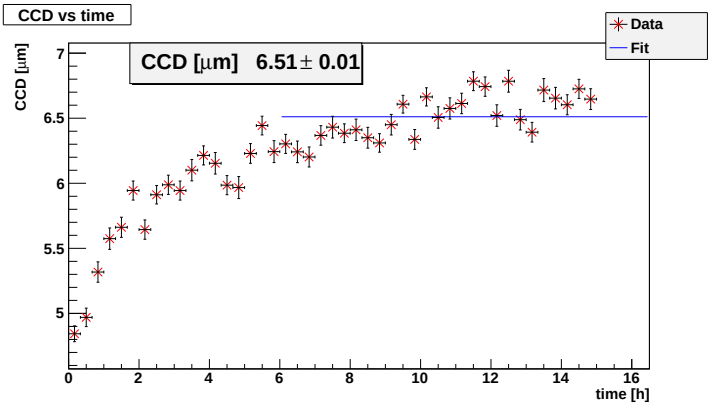


***Figure A.23.:*** Measurement of CCD of diamond sample 2 over time at a bias voltage of 100 V. Only statistical errors are shown.

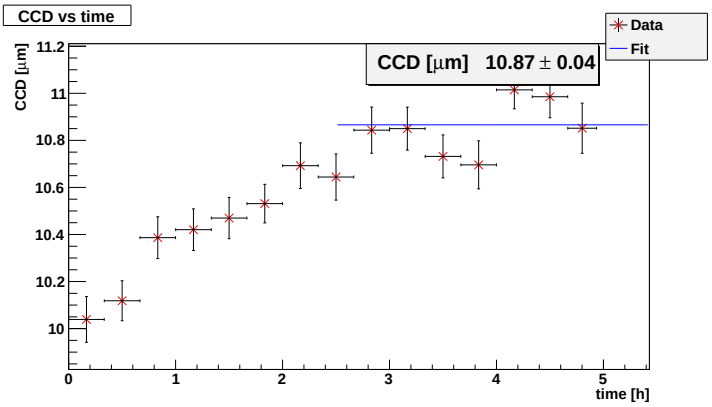


***Figure A.24.:*** Measurement of CCD of diamond sample 2 over time at a bias voltage of 200 V. Only statistical errors are shown.

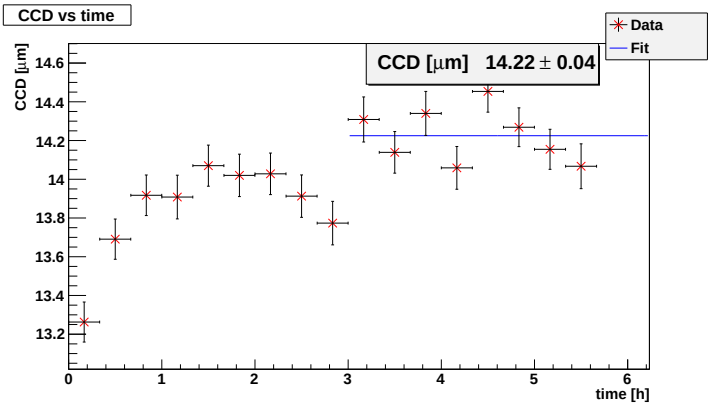


***Figure A.25.:*** Measurement of CCD of diamond sample 2 over time at a bias voltage of 300 V. Only statistical errors are shown.

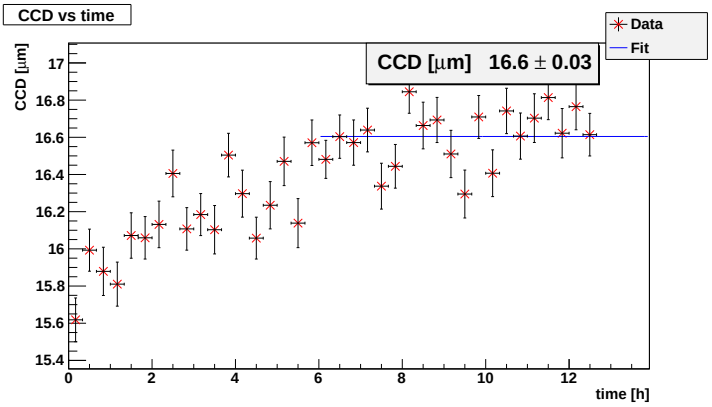


***Figure A.26.:*** Measurement of CCD of diamond sample 2 over time at a bias voltage of 400 V. Only statistical errors are shown.

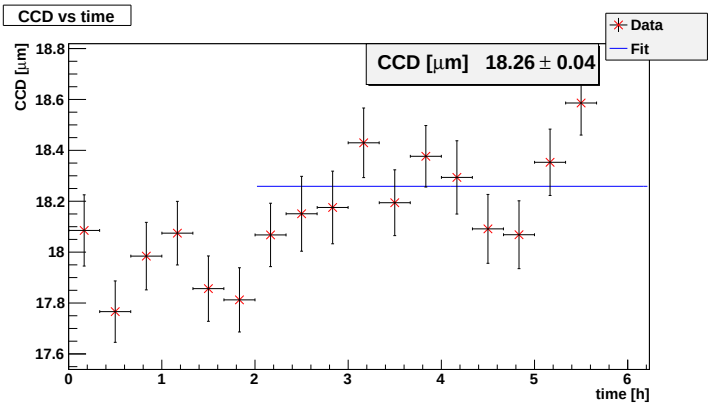


***Figure A.27.:*** Measurement of CCD of diamond sample 2 over time at a bias voltage of 500 V. Only statistical errors are shown.

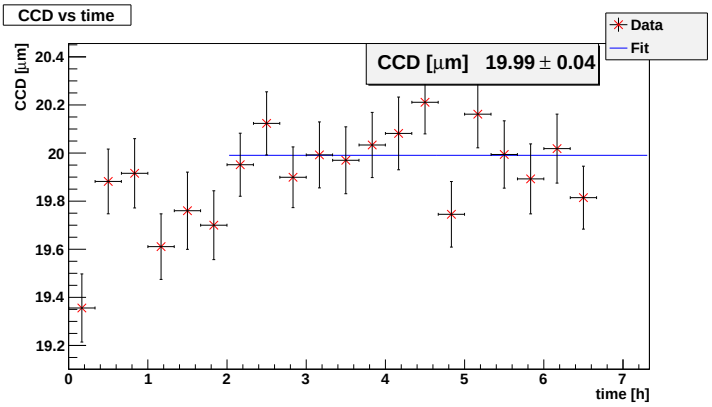


***Figure A.28.:*** Measurement of CCD of diamond sample 2 over time at a bias voltage of 600 V. Only statistical errors are shown.

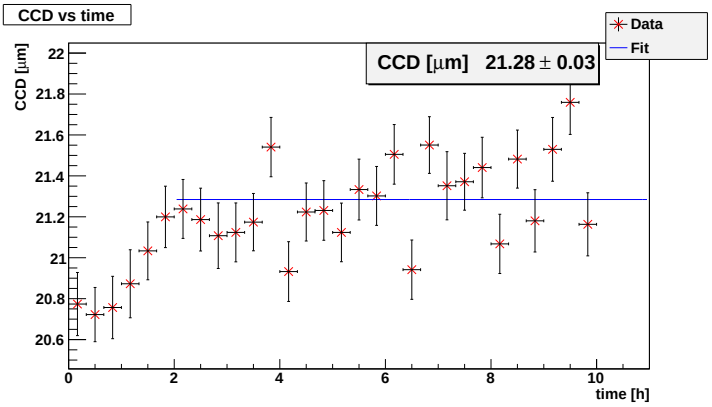


***Figure A.29.:*** Measurement of CCD of diamond sample 2 over time at a bias voltage of 700 V. Only statistical errors are shown.

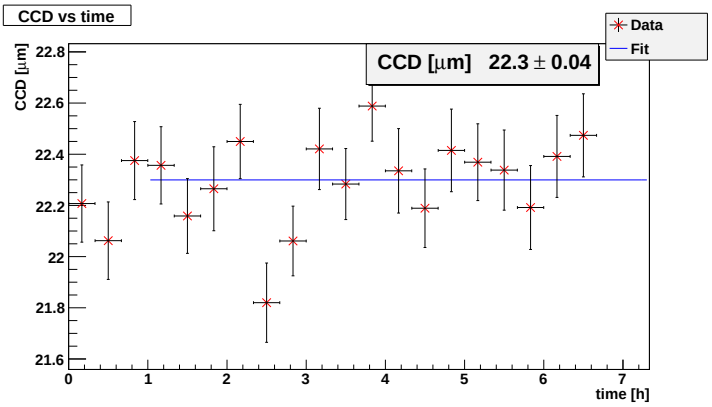


***Figure A.30.:*** Measurement of CCD of diamond sample 2 over time at a bias voltage of 800 V. Only statistical errors are shown.

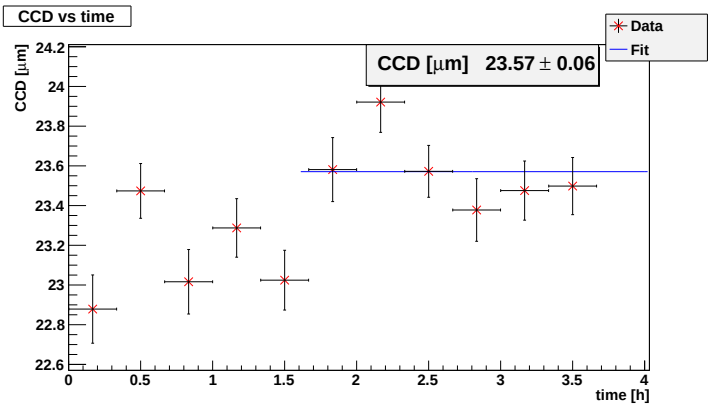


***Figure A.31.:*** Measurement of CCD of diamond sample 2 over time at a bias voltage of 900 V. Only statistical errors are shown.

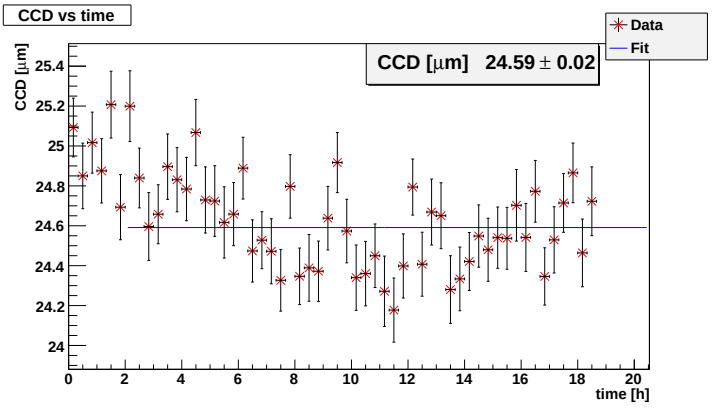


***Figure A.32.:*** Measurement of CCD of diamond sample 2 over time at a bias voltage of 1000 V. Only statistical errors are shown.

# Bibliography


[1] K. Kleinknecht, *Detektoren für Teilchenstrahlung*, Teubner (2005)

[2] W. R. Leo, *Techniques for Nuclear and Particle Physics Experiments: A How-to Approach*, Springer-Verlag (1994)

[3] K. Nakamura et al., *The Review of Particle Physics*, J. Phys. G **37**, 075021 (2010)

[4] J. Große-Knetter, *Vertex Measurment at a Hadron Collider - The ATLAS Pixel Detector*, Habilitation, Bonn University (2008)

[5] H. Pernegger, *High mobility diamonds and particle detectors*, Physica Status Solidi (a) **203(13)**, 3299 (2006)

[6] S. Ramo, *Currents Induced by Electron Motion*, Proceedings of the IRE **27(9)**, 584 (1939)

[7] F. P. Bundy et al., *Man-Made Diamonds*, Nature **176(4471)**, 51 (1955)

[8] H. T. Hall, *Ultrahigh-Pressure Research*, Science **128(3322)**, 445 (1958)

[9] K. L. Choy, *Chemical vapour deposition of coatings*, Progress in Materials Science **48(2)**, 57 (2003)

[10] C. Bauer et al., *Radiation hardness studies of CVD diamond detectors*, Nucl. Inst. and Meth. A **367(1-3)**, 207 (1995), Proceedings of the 7th International Wire Chamber Conference

[11] M. Capeans et al., *ATLAS Insertable B-Layer Technical Design Report*, Technical Report CERN-LHCC-2010-013. ATLAS-TDR-019, CERN, Geneva (2010)

[12] O. S. Brüning et al., *LHC Luminosity and energy upgrade: A Feasibility Study*, Technical Report LHC-Project-Report-626. CERN-LHC-Project-Report-626, CERN, Geneva (2002)

[13] G. Lutz, *Semiconductor radiation detectors: device physics*, Springer Verlag (2007)

[14] D. K. Schroder, *Semiconductor material and device characterization*, Wiley-IEEE Press (2006)

[15] H. Spieler, *Semiconductor Detector Systems*, Oxford University Press (2005)

[16] D. Asner et al., *Diamond pixel modules*, Nucl. Inst. and Meth. A **636(1, Supplement 1)**, S125 (2011), 7th International Hiroshima Symposium on the Development and Application of Semiconductor Tracking Detectors

[17] T. Rohe et al., *Sensor design for the ATLAS-pixel detector*, Nucl. Inst. and Meth. A **409**, 224 (1998)

[18] S. I. Parker et al., *3D – A proposed new architecture for solid-state radiation detectors*, Nucl. Inst. and Meth. A **395(3)**, 328 (1997), Proceedings of the Third International Workshop on Semiconductor Pixel Detectors for Particles and X-rays

[19] C. D. Via et al., *Advances in silicon detectors for particle tracking in extreme radiation environments*, Nucl. Inst. and Meth. A **509(1-3)**, 86 (2003), Proceedings of the 4th Internatonal Workshop on Radiation Imaging Detectors

[20] S. I. Parker, C. J. Kenney, *Performance of 3-D architecture silicon sensors after intense proton irradiation*, IEEE Transactions on Nuclear Science **48(5)**, 1629 (2001)

[21] M. Mathes, *Development and characterization of diamond and 3D-silicon pixel detectors with ATLAS-pixel readout electronics*, Ph.D. thesis, Universitäts-und Landesbibliothek Bonn (2008)

[22] G. Pellegrini et al., *Technology development of 3D detectors for high-energy physics and imaging*, Nucl. Inst. and Meth. A **487(1-2)**, 19 (2002)

[23] J. Qian et al., *Partial graphitization of diamond crystals under high-pressure and high-temperature conditions*, Journal of Applied Physics **90(3)**, 1632 (2001)

[24] J. Qian et al., *Graphitization of diamond powders of different sizes at high pressure-high temperature*, Carbon **42(12-13)**, 2691 (2004)

[25] V. R. Howes, *The Graphitization of Diamond*, Proceedings of the Physical Society **80(3)**, 648 (1962)

[26] S. Talapatra et al., *Ion irradiation induced structural modifications in diamond nanoparticles*, Nanotechnology **17(1)**, 305 (2006)

[27] D. Saada et al., *Computer simulation of damage in diamond due to ion impact and its annealing*, Phys. Rev. B **59(10)**, 6650 (1999)

[28] A. Sorkin et al., *Computer simulations of damage due to passage of a heavy fast ion through diamond*, Phys. Rev. B **70(6)**, 064110 (2004)

[29] S. Prawer, R. Kalish, *Ion-beam-induced transformation of diamond*, Phys. Rev. B **51(22)**, 15711 (1995)

[30] B. Miller et al., *Patterned Electrical Conductance and Electrode Formation in Ion-Implanted Diamond Films*, Journal of The Electrochemical Society **141(4)**, L41 (1994)

[31] J. Krauser et al., *Ion track lithography and graphitic nanowires in diamondlike carbon*, J. Vac. Sci. Technol. **26(6)**, 2468 (2008)

[32] T. Kononenko et al., *Microstructuring of diamond bulk by IR femtosecond laser pulses*, Applied Physics A: Materials Science & Processing **90**, 645 (2008)

[33] M. Neff et al., *Femtosecond laser writing of buried graphitic structures in bulk diamond*, Applied Physics A: Materials Science & Processing **97**, 543 (2009)

[34] T. Kononenko et al., *Three-dimensional laser writing in diamond bulk*, Diamond and Related Materials **20(2)**, 264 (2011)

[35] K. Okada, T. Sekino, *Agilent Technologies Impedance Measurement Handbook July 2006*, July, Agilent Technologies (2006)

[36] Agilent Technologies, *Agilent B1500A Semiconductor Device Analyzer - User's Guide*, 7. edition (2008)

[37] Fast ComTech GmbH, *CSP10 User Manual* (2009)

[38] J.-W. Tsung, private communication

[39] I. N. Bronstein et al., *Handbuch der Mathematik*, Verlag Harri Deutsch (2008)

# Danksagung

Ich möchte Prof. Dr. Arnulf Quadt für die Möglichkeit danken in seiner Arbeitsgruppe diese Masterarbeit anfertigen zu können.
Ebenso gilt mein Dank meinem Betreuer Dr. Jens Weingarten, der mich stets unterstützt hat und mir hilfreich zur Seite stand.
Auch Prof. Dr. Claus Ropers möchte ich für den Zugang zu einem Femtosekundenlaser danken, sowie Max Gulde für die technische Unterstützung bei dieser Messung.
Für das Korrekturlesen dieser Arbeit danke ich Jens und Nina.
Zum Schluss gilt mein Dank meinen Eltern, die mir ein sorgenfreies Studium ermöglicht haben.

**Erklärung** nach §18(8) der Prüfungsordnung für den Bachelor-Studiengang Physik und den Master-Studiengang Physik an der Universität Göttingen:

Hiermit erkläre ich, dass ich diese Abschlussarbeit selbständig verfasst habe, keine anderen als die angegebenen Quellen und Hilfsmittel benutzt habe und alle Stellen, die wörtlich oder sinngemäß aus veröffentlichten Schriften entnommen wurden, als solche kenntlich gemacht habe.
Darüberhinaus erkläre ich, dass diese Abschlussarbeit nicht, auch nicht auszugsweise, im Rahmen einer nichtbestandenen Prüfung an dieser oder einer anderen Hochschule eingereicht wurde.

Göttingen, den 8. September 2011

(Lars Graber)